Contents

List of Figures

Chapter 2

Integer Quantum Hall Effect

2.1 Continuum Percolation

2.1.1 Dynamics in the LLL

Recall the classical equation of motion for an electron in a field $\boldsymbol{B}$ subject to a potential $V(\boldsymbol{r})$,

$$m\ddot{\boldsymbol{r}} = -\boldsymbol{\nabla} V - \frac{e}{c}\,\dot{\boldsymbol{r}} \times \boldsymbol{B} \quad . \tag{2.1}$$

Averaging over the fast classical cyclotron motion $\boldsymbol{\xi}(t)$, we obtained the dynamics of the guiding-center $\boldsymbol{\mathcal{R}}(t)$,

$$\frac{d\boldsymbol{\mathcal{R}}}{dt} = \frac{\ell^2}{\hbar}\,\hat{\boldsymbol{z}} \times \boldsymbol{\nabla} V_{\rm eff}(\boldsymbol{\mathcal{R}}) \quad , \tag{2.2}$$

where the effective potential is $V_{\rm eff}(\boldsymbol{\mathcal{R}}) = V(\boldsymbol{\mathcal{R}}) + \frac{1}{2}\langle \boldsymbol{\xi}^2 \rangle\, \nabla^2 V(\boldsymbol{\mathcal{R}}) + \ldots$, and where we have taken $\boldsymbol{B} = -B\hat{\boldsymbol{z}}$. Thus, $dV_{\rm eff}\big(\boldsymbol{\mathcal{R}}(t)\big)/dt = 0$ and the guiding-center moves along an equipotential.

At the quantum level, recall how in chapter 1 we derived the LLL-projected potential,

$$\widetilde{V}(\boldsymbol{\mathcal{R}}) = \langle\, 0 \,|\, V \,|\, 0 \,\rangle = \int \frac{d^2k}{(2\pi)^2}\, \hat{V}(\boldsymbol{k})\, e^{i\boldsymbol{k}\cdot\boldsymbol{\mathcal{R}}}\, e^{-\boldsymbol{k}^2\ell^2/4} = \big(1 + \tfrac{1}{4}\,\ell^2\,\nabla^2 + \ldots\big) V(\boldsymbol{\mathcal{R}}) \quad , \tag{2.3}$$

where $\boldsymbol{\mathcal{R}}$ is the guiding-center position operator, the Cartesian components of which satisfy $[\mathcal{X}, \mathcal{Y}] = -i\ell^2$. Thus we have the equivalences

$$\mathcal{X} = \frac{\ell^2}{i}\,\frac{\partial}{\partial \mathcal{Y}} \qquad , \qquad \mathcal{Y} = i\ell^2\,\frac{\partial}{\partial \mathcal{X}} \quad . \tag{2.4}$$

Thus the Ehrenfest equations of motion are

$$\frac{d\langle \mathcal{X} \rangle}{dt} = -\frac{\ell^2}{\hbar}\,\Big\langle\, \frac{\partial \widetilde{V}}{\partial \mathcal{Y}} \,\Big\rangle \qquad , \qquad \frac{d\langle \mathcal{Y} \rangle}{dt} = +\frac{\ell^2}{\hbar}\,\Big\langle\, \frac{\partial \widetilde{V}}{\partial \mathcal{X}} \,\Big\rangle \quad . \tag{2.5}$$

At the semiclassical level, we remove the brackets, replace $\langle \mathcal{X} \rangle \to X$ and $\langle \mathcal{Y} \rangle \to Y$, and write $\dot{X} = -\frac{\ell^2}{\hbar}\frac{\partial \widetilde{V}}{\partial Y}$ and $\dot{Y} = +\frac{\ell^2}{\hbar}\frac{\partial \widetilde{V}}{\partial X}$. We can reproduce these results from the coherent state path integral approach. Recall that the complexified guiding-center position operator is $\mathcal{R} = \sqrt{2}\,\ell b^\dagger$, hence the coherent state path integral action is given by Eqn. 1.278, replacing $z = \bar{R}/\sqrt{2}\,\ell$, *i.e.*

$$\mathcal{S}\big[\{R(t), \bar{R}(t)\}\big]/\hbar = \int_0^T dt \left\{ \frac{1}{4i\ell^2}\left(\bar{R}\,\frac{dR}{dt} - R\,\frac{d\bar{R}}{dt}\right) - \frac{1}{\hbar}\,\widetilde{V}(R\,|\bar{R})\right\} + \Delta\mathcal{S}/\hbar \quad , \tag{2.6}$$

where

$$\Delta\mathcal{S} = \frac{i\hbar}{4\ell^2}\Big(R_{\rm f}\big[\bar{R}_{\rm f} - \bar{R}(T)\big] - \bar{R}_{\rm i}\big[R(0) - R_{\rm i}\big]\Big) \quad . \tag{2.7}$$

is the boundary discontinuity term, which does not affect the equations of motion. Taking the functional variation with respect to R and $\bar{R}$ yields the complexified equations of motion,

$$\frac{dR}{dt} = \frac{2i\ell^2}{\hbar}\,\frac{\partial \widetilde{V}(R\,|\bar{R})}{\partial \bar{R}} \quad , \qquad \frac{d\bar{R}}{dt} = -\frac{2i\ell^2}{\hbar}\,\frac{\partial \widetilde{V}(R\,|\bar{R})}{\partial R} \quad , \tag{2.8}$$

which are indeed the complexified forms of

$$\dot{X} = -\frac{\ell^2}{\hbar}\,\frac{\partial \widetilde{V}}{\partial Y} \quad , \qquad \dot{Y} = +\frac{\ell^2}{\hbar}\,\frac{\partial \widetilde{V}}{\partial X} \quad . \tag{2.9}$$

In vectorized form, $\dot{\boldsymbol{R}} = \hbar^{-1}\ell^2\,\hat{\boldsymbol{z}} \times \boldsymbol{\nabla}\widetilde{V}$.

2.1.2 Electrons in a smooth random potential

In heterojunction inversion layers, the potential $\widetilde{V}(\boldsymbol{R})$ arises from the electrical potential due to the recessed donor ions (Si^+ substituting for Al in $Al_xGa_{1-x}As$). While the displacement of the Si^+ dopant ions in the direction ($\hat{\boldsymbol{z}}$) perpendicular to the inversion layer is rather precisely controlled ("δ-doping"), they are located pretty much randomly in the (x, y) plane, hence the potential may be taken to be random, though smoothed out on a scale on the order of the distance between the GaAs-$Al_xGa_{1-x}As$ interface and the dopant layer, which is typically several hundreds of Ångstroms. Landau level projection further smooths the potential by further suppressing high spatial frequencies via the $\exp(-\boldsymbol{k}^2\ell^2/4)$ factor. A mock-up of such a smooth random potential is shown in Fig. 2.1. One can generate such $\widetilde{V}\boldsymbol{R})$ from a distribution functional

$$P\big[\widetilde{V}(\boldsymbol{R})\big] = P[0]\,\exp\left\{-\frac{1}{2\gamma}\int d^2R\,\Big[\widetilde{V}^2 + \lambda^2\big(\boldsymbol{\nabla}\widetilde{V}\big)^2\Big]\right\} \quad , \tag{2.10}$$

where $P[0]$ ensures normalization of the functional integral $\int D\widetilde{V}\,P\big[\widetilde{V}\big] = 1$. Here, λ is the length scale over which $\widetilde{V}(\boldsymbol{R})$ is correlated. Indeed, for the above distribution functional, the

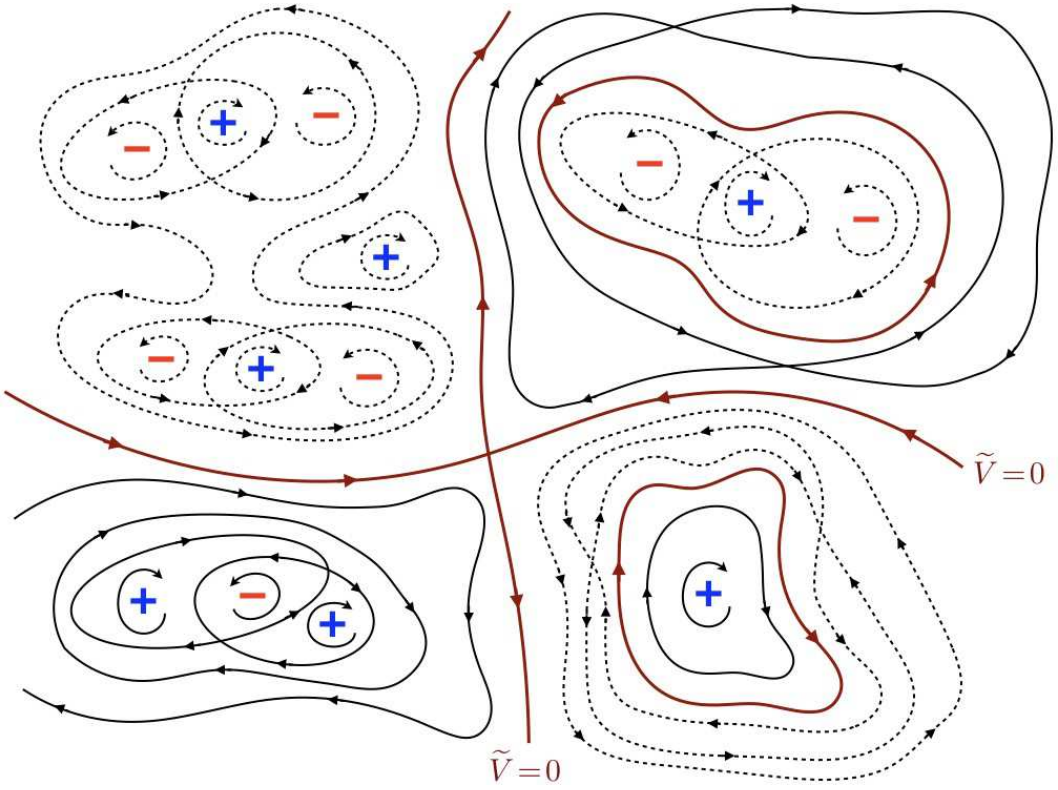

Figure 2.1: Contour plots for a symmetrically random potential $\widetilde{V}(\boldsymbol{R})$. Electrons move clockwise around peaks (+) and counterclockwise around valleys (−). Solid lines indicate level sets with $\widetilde{V}(\boldsymbol{R}) > 0$; dashed lines correspond to $\widetilde{V}(\boldsymbol{R}) < 0$. The brown curves lie at $\widetilde{V}(\boldsymbol{R}) = 0$, which is the continuum percolation threshold.

correlation function is of the two-dimensional Ornstein-Zernike form,

$$\left\langle \widetilde{V}(\boldsymbol{R})\,\widetilde{V}(\boldsymbol{0})\right\rangle = \frac{\gamma}{2\pi\lambda^2}\,K_0(R/\lambda) \quad , \tag{2.11}$$

where $K_0(z)$ is the Hankel function of imaginary argument[1], whose asymptotic behavior is

$$K_0(z) = \begin{cases} -\ln z + \ln 2 - \mathsf{C} + \mathcal{O}(z^2 \ln z) & z \to 0 \\ (\pi/2z)^{1/2}\exp(-z) \times \left\{1 + \mathcal{O}(z^{-1})\right\} & z \to \infty \end{cases} \quad , \tag{2.12}$$

where $\mathsf{C} = 0.57721\ldots$ is the Euler-Mascheroni constant. The divergence as $R \to 0$ can be cured by imposing a cutoff at high spatial frequency $k = \Lambda$, rendering $\left\langle \widetilde{V}^2(\boldsymbol{0})\right\rangle$ finite.

The equipotentials (*i.e.* the level sets) of a given random $\widetilde{V}(\boldsymbol{R})$ will appear as in Fig. 2.1, with peaks, valleys, and saddle points. The LLL dynamics in a field $\boldsymbol{B} = -B\hat{\boldsymbol{z}}$ are such that electrons circle clockwise around peaks and counterclockwise around valleys, as depicted in the figure.

[1]See Gradshteyn and Ryzhik §8.4.

For symmetrically distributed $\widetilde{V}(\boldsymbol{R})$, there will be a unique value $\widetilde{V}(\boldsymbol{R}) = 0$ where the level set is of infinite continuous extent. Electrons with energies $\widetilde{V} = 0$ can percolate across the entire sample, which is an infinite distance in the thermodynamic limit.

Semiclassically, the LLL electron wavefunctions are localized along the equipotentials. Recall the wavefunctions in the symmetric gauge and in the absence of a potential are given by $\psi_m(\boldsymbol{r}) = C_m\, z^m \exp(-|z|^2/4\ell^2)$. Maximizing $\psi_m(\boldsymbol{r})|^2$, one finds $r_m^2 = 2m\ell^2$, which is a ring enclosing an area $A_m = 2\pi m\ell^2$. Thus, increasing m by $\Delta m = 1$ is associated with a concomitant increase in area by the quantum $2\pi\ell^2$. The semiclassical wavefunctions obey the same quantization rule $A_m = 2\pi m\ell^2$, except they are localized along equipotentials of $\widetilde{V}(\boldsymbol{r})$ rather than along circles. If we parameterize an equipotential curve $\widetilde{V}(\boldsymbol{r}) = E_{\rm F}$ by a distance u along the curve and a distance v locally perpendicular to it, then the semiclassical eigenfunctions, following Trugman[2], take the form

$$\psi(u,v) = |\boldsymbol{\nabla}\widetilde{V}(u,0)|^{-1/2}\, H_n(v/\ell)\, \exp(-v^2/2\ell^2)\, e^{i\chi(u,v)} \quad , \tag{2.13}$$

where $\chi(u,v)$ is a gauge-dependent phase function whose winding around the equipotential increases by 2π with each consecutive semiclassical energy eigenstate. Here we have included the LL index n; note that this is essentially the Landau strip wavefunction written in local coordinates (u,v). It is valid provided $\ell \ll b$ where b is the local radius of curvature of the contour, and if $|\boldsymbol{\nabla}\widetilde{V}| \ll \hbar\omega_{\rm c}/\ell$. Because electrons are fermions, these semiclassical levels will be filled up to the Fermi energy. The contour at $\widetilde{V}(\boldsymbol{r}) = E_{\rm F}$ represents the highest occupied electronic energy level. The following vivid analogy may be helpful:

> *Imagine $\widetilde{V}(\boldsymbol{r})$ is the height function of a random landscape. After a long period of rain, every part of the landscape for which $\widetilde{V}(\boldsymbol{r}) < E_{\rm F}$ is under water. You are constrained to walk in such a way that your left foot is always under water, and your right foot is always on dry land.*

When the Fermi level $E_{\rm F}$ is low, you are constrained to walk in a counterclockwise direction (as viewed from above) about isolated puddles. When the Fermi level $E_{\rm F}$ is high, you are constrained to walk in a clockwise direction around isolated islands. In each case, you don't get very far from wherever you started. Now you know what a classical electron in a random potential and a large magnetic field feels like.

For a given realization $\widetilde{V}(\boldsymbol{r})$ of the random potential, the density of level sets, per unit energy, is given by

$$\rho(E) = \frac{1}{A}\int d^2r\, \delta\big(E - \widetilde{V}(\boldsymbol{r})\big) \quad , \tag{2.14}$$

where A is the total area. The electronic density of states[3] is $g(E) = N_\phi^{-1}\sum_m \delta(E - E_m)$, where m is an eigenstate label within the LLL. In the limit $B \to \infty$, we have $g(E) = \rho(E)$, which is

[2] See S. A. Trugman, *Phys. Rev. B* **27**, 7539 (1983).

[3] Here $g(E)$ is defined to be the DOS per unit energy per unit flux.

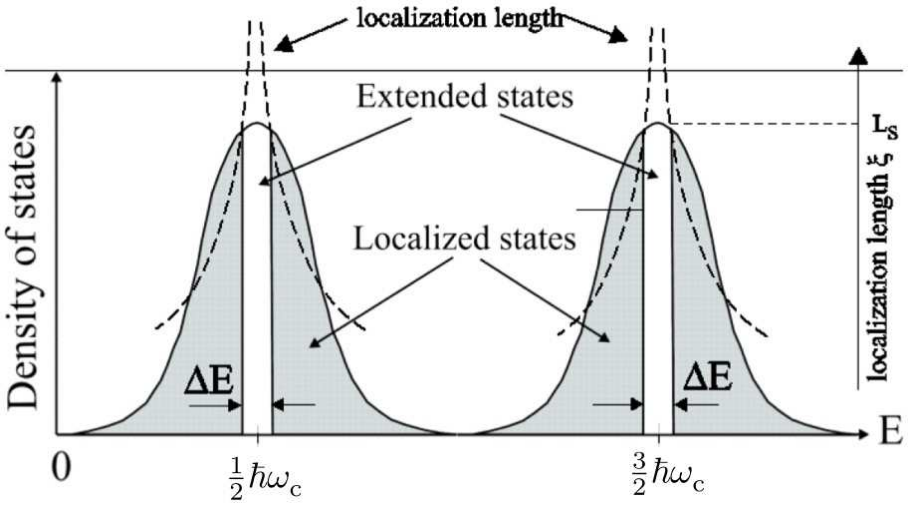

Figure 2.2: Density of states, correlation length, and mobility gaps in disorder-broadened Landau levels. In the thermodynamic limit, extended states exist only at unique energies corresponding to the (quantum) continuum percolation threshold at the centers of each Landau level. For systems of finite linear dimension L, a range of states with $\xi(E) > L$ may be considered as extended. *Image: J. Oswald, DOI:10.5772/62926.*

to say that each eigenstate is associated with a quantum of area $2\pi\ell^2$. Note the normalization condition $\int_{-\infty}^{\infty} dE\, \rho(E) = \int_{-\infty}^{\infty} dE\, g(E) = 1$. We are interested in the properties of the eigenstates as a function of their energy E. In particular, what is their typical spatial extent? Let the standard deviation of the random potential be $\Delta = \left\langle \widetilde{V}^2(\mathbf{0}) \right\rangle^{1/2}$. For E/Δ sufficiently negative, only the lowest valleys will support occupied electronic states. Similarly, for E/Δ sufficiently positive, only the highest peaks will support *unoccupied* electronic states. As $|E|$ decreases, the spatial extent of the equipotentials $\widetilde{V}(\boldsymbol{r}) = E$ increases. If $\widetilde{V}(\boldsymbol{r})$ is symmetrically distributed, then there will be a unique critical energy $E_c = 0$ at which the typical size of the equipotentials diverges, as $\xi(E) \propto |E|^{-\nu}$, where $\nu = \frac{4}{3}$ is the correlation length exponent for two-dimensional *percolation*.

2.1.3 Percolation theory

Percolation is a geometric critical phenomenon describing the clustering and the emergence of an infinite connected network in random systems[4]. We first describe the setting for *site percolation*. Consider a lattice in which each site is randomly occupied with probability $p \in [0, 1]$. One defines a *cluster* as a maximal connected set of occupied sites[5]. An *s-cluster* is defined to be a cluster of size s. The probability that a given site belongs to a cluster of *infinite* extent is

[4]See, *e.g.*, D. Stauffer, *Phys. Reg.* **54**, 1 (1979) and J. W. Essam, *Rep. Prog. Phys.* **43**, 53 (1980).
[5]Maximal in the sense that all occupied sites connected to the cluster are accounted to be in the cluster.

called the *percolation probability*, $P_\infty \equiv P(p)$. The *percolation threshold* is the largest value of p for which $P(p) = 0$. For $p < p_{\rm c}$ one has $P(p) = 0$, but for $p - p_{\rm c}$ small and positive, $P(p) \propto (p - p_{\rm c})^\beta$, where β is a critical exponent. Just as in a magnetic system, where the order parameter is the magnetization $\boldsymbol{M}(T) \propto (T_{\rm c} - T)_+^\beta$, in percolation theory the order parameter is $P(p)$[6].

Let $n_s(p)$ be the number of s-clusters per lattice site. Then for each lattice site there are three possibilities: (i) the site may be unoccupied, with probability $1-p$, (ii) the site may be occupied and a member of a finite cluster of size s, with probability n_s, or (iii) the site may be occupied and a member of an infinite cluster, with probability $p\,P(p)$. Thus,

$$(1-p) + \sum_{s=1}^{\infty} s\,n_s(p) + p\,P(p) = 1 \quad . \tag{2.15}$$

Note that this entails $\sum_{s=1}^\infty s\,n_s(p) = p\big(1 - P(p)\big)$. Examples of percolation clusters on are depicted in Fig. 2.3 for the square lattice[7]. As an application, consider a dilute Ising magnet at temperatures $T \ll J/k_{\rm B}$, where J is the exchange energy. The magnetization $M(T, H, p)$ is given by

$$M(T, H, p) = \pm P(p) + p^{-1} \sum_{s=1}^{\infty} s\,n_s(p)\,\tanh(s\mu H/k_{\rm B}T) \quad . \tag{2.16}$$

For $p < p_{\rm c}$, only finite clusters are present, and there is zero magnetization at $H = 0$. For $p > p_{\rm c}$, there is an infinite cluster, which immediately polarizes for any finite H. In thermodynamic equilibrium, we have $\pm P(p) = P(p)\,\mathrm{sgn}(H)$, but it may be that the infinite cluster gets stuck in a metastable state, *i.e.* that there is hysteresis. Another application of percolation theory is to the properties of random mixtures of conducting and nonconducting elements, such as aluminum and glass marbles, or random resistor networks[8].

In the vicinity of $p = p_{\rm c}$, the following critical properties pertain:

$$\begin{aligned} \sum_{s=1}^{\infty} n_s(p) &\propto |p - p_{\rm c}|^{2-\alpha} + \text{nst} \quad , \quad \sum_{s=1}^{\infty} s\,n_s(p) \propto (p - p_{\rm c})_+^\beta + \text{nst} \\ \sum_{s=1}^{\infty} s^2\,n_s(p) &\propto |p - p_{\rm c}|^{-\gamma} + \text{nst} \quad , \quad \sum_{s=1}^{\infty} s\,n_s(p_{\rm c})\,e^{-hs} \propto h^{1/\delta} + \text{nst} \quad , \end{aligned} \tag{2.17}$$

with the 'field' h small and positive, and where "nst" means "non-singular terms". One also defines the *correlation length* $\xi(p)$ to be the typical diameter of finite clusters. Let $g(\boldsymbol{r}, p)$ be

[6] We define $x_+ \equiv x\,\Theta(x)$.

[7] One might think that if the set of occupied sites does not percolate, *i.e.* if $p < p_{\rm c}$, that the unoccupied sites must percolate, but this is false. Clearly on any bipartite lattice if all the A sublattice sites are occupied and all the B sublattice sites are unoccupied, then *neither* the occupied nor the unoccupied sites percolates. Indeed in this example the only clusters are of size $s = 1$.

[8] See, *e.g.* S. Kirkpatrick, *Rev. Mod. Phys.* **45**, 574 (1973).

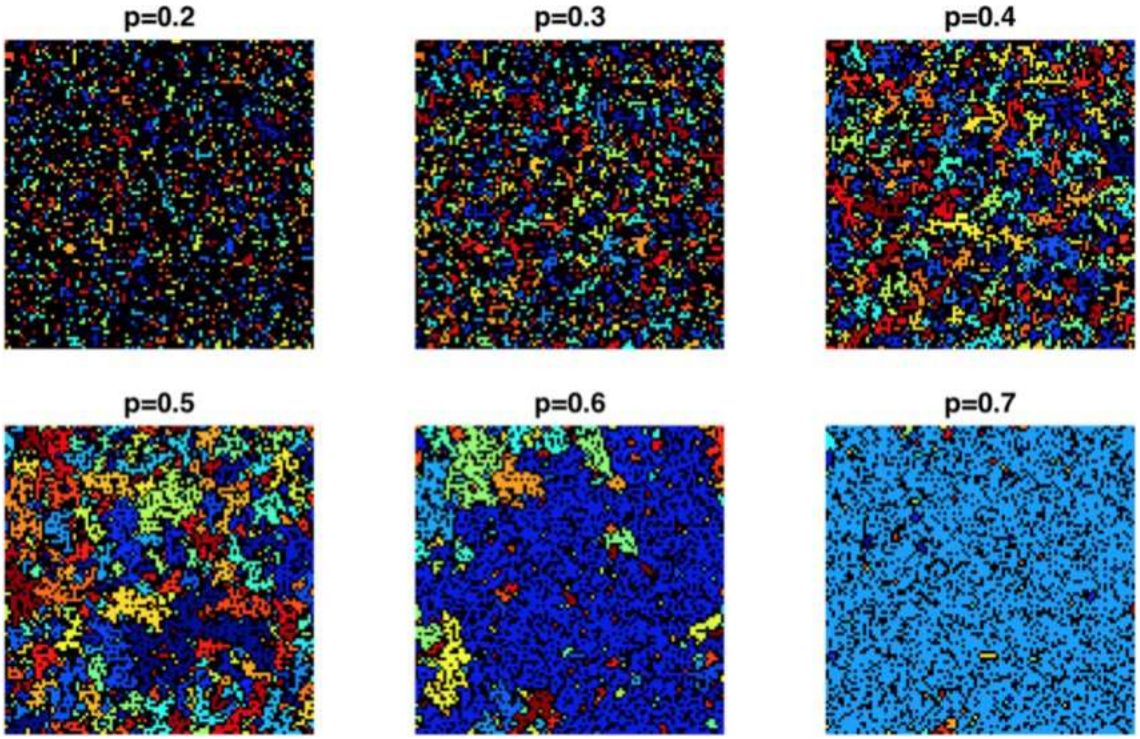

Figure 2.3: Site percolation clusters on the square lattice ($p_c \simeq 0.5927$). Each distinct cluster appears as a different color. Unoccupied sites are shown in black. The infinite cluster for $p = 0.7$ is shown in light blue. From A. Malthe-Sorenssen, *Percolation and Disordered Systems – A Numerical Approach* (unpublished, 2015).

the *pair connectivity function*, defined as the probability that two occupied sites separated by a distance $\boldsymbol{r}$ belong to the same finite cluster. One then has

$$\xi^2(p) = \frac{\sum_{\boldsymbol{r}} \boldsymbol{r}^2 g(\boldsymbol{r}, p)}{\sum_{\boldsymbol{r}} g(\boldsymbol{r}, p)} \quad . \tag{2.18}$$

The scaling hypothesis

Following Stauffer, in the vicinity of $p = p_c$, we adopt a scaling *Ansatz* which says that the critical behavior is dominated by clusters of size $s_\xi \propto |p - p_c|^{-1/\sigma}$, where σ is a universal critical exponent. Precisely at $p = p_c$, the singular part of the cluster size distribution is presumed to behave as $n(p_c) \propto s^{-\tau}$, where τ is another universal critical exponent. Thus, the scaling hypothesis entails the relation $n_s(p) = n_s(p_c)\, \phi(s/s_\xi)$ with $\phi(0) = 1$, *i.e.*

$$n_s(p) \propto s^{-\tau} \phi_\pm\big(|p - p_c|^{1/\sigma} s\big) \quad , \tag{2.19}$$

where the $\pm$ sign is for $p \gtrless p_c$. It is important to understand that s_ξ is the cluster size which dominates in the *singular part* of $\sum_{s=1}^{\infty} s\, n_s(p)$; the smooth contributions are dominated by much

d	α	β	γ	δ	η	ν	σ	τ	$d_{\rm f}$
2	$-2/3$	$5/36$	$43/18$	$91/5$	$5/24$	$4/3$	$36/91$	$187/91$	$91/48$
3	$-0.625(3)$	$0.418(1)$	$1.805(2)$	$5.29(6)$	$-0.059(9)$	$0.875(1)$	$0.445(1)$	$2.190(2)$	$2.530(1)$
4	$-0.756(4)$	$0.657(9)$	$1.435(1)$	$3.198(6)$	$-0.0929(9)$	$0.689(1)$	$0.476(5)$	$2.313(3)$	$3.056(7)$

Table 2.1: Critical exponents for percolation. η is the anomalous exponent describing the power law decay of correlations at criticality, and $d_{\rm f}$ is the fractal dimension of the percolation cluster. For $d > 2$, there is some variation reported in numerical computations of the critical exponents. *Source: Wikipedia (Percolation Critical Exponents).*

smaller clusters. If we further define $g_{s,t}$ to be the number of distinct cluster configurations with total size s and perimeter t, then the average number of s-clusters with perimeter t is given by $n_{s,t}(p) = g_{s,t}\, p^s\, (1-p)^t$. An analog for the partition function can be defined for the percolation problem, *viz.*[9]

$$Z(p,h) = \sum_{s=1}^{\infty}\sum_{t=1}^{\infty} g_{s,t}\, p^s\, q^t\, e^{-ht} = \sum_{s=1}^{\infty}\sum_{t=1}^{\infty} n_{s,t}(p)\, e^{-ht} \quad , \tag{2.20}$$

where $q = 1-p$. Writing $Z_s(p,h) = \sum_t g_{s,t}\, q^t\, e^{-ht}$, one has

$$t_s(p) = \frac{\sum_t t\, n_{s,t}(p)}{\sum_t n_{s,t}(p)} = \frac{\partial \ln Z_s(p, h=0)}{\partial \ln q} = \frac{qs}{p} - q\,\frac{\partial \ln n_s(p)}{\partial p} \quad . \tag{2.21}$$

For large s, the second term is known to behave as s^ζ with $\zeta < 1$, hence in the large s limit we have $t_s = (p^{-1}-1)\, s \propto s$. Thus, the large clusters are highly ramified, with $t_s \sim s$. Note that summing $n_{s,t}(p)$ over the perimeter t gives $n_s(p) = \sum_t n_{s,t}(p)$.

From the scaling relations, we may obtain all the critical exponents in terms of σ and τ. For example,

$$\sum_{s=1}^{\infty} s\, n_s(p) \sim \int_1^{\infty} ds\; s^{1-\tau}\, \phi_\pm\big(|\delta p|^{1/\sigma} s\big) \sim \int_{|\delta p|^{1/\sigma}}^{\infty} du\; e^{1-\tau}\, \phi(u) \cdot |\delta p|^{(\tau-2)/\sigma} \propto (\delta p)_+^{\beta} \tag{2.22}$$

where $\delta p \equiv p - p_{\rm c}$. Thus we conclude $\beta = (\tau-2)/\sigma$. Similarly,

$$\sum_{s=1}^{\infty} s\, n_s(p_{\rm c}) e^{-hs} \sim \int_1^{\infty} ds\; s^{1-\tau}\, \phi(0)\, e^{-hs} \sim \phi(0) \int_h^{\infty} du\; u^{1-\tau}\, e^{-u} \cdot h^{2-\tau} \propto h^{1/\delta} \tag{2.23}$$

whence $\delta = 1/(\tau-2)$. The full set of exponents is given by

$$\alpha = 2 + \frac{1-\tau}{\sigma} \quad , \quad \beta = \frac{\tau-2}{\sigma} \quad , \quad \gamma = \frac{3-\tau}{\sigma} \quad , \quad \delta = \frac{1}{\tau-2} \quad . \tag{2.24}$$

[9] Note that the minimum value t can take for nonzero $g_{s,t}$ is $t = z$, the lattice coordination number.

Finally, assuming hyperscaling, which is to say that the singular part of the free energy density scales as $\big[\xi(p)\big]^{-d}$, one may derive the correlation length exponent $\nu = (\tau-1)/\sigma d$. Values for the critical exponents is $d = 2, 3, 4$ are listed in Tab. 2.1. For reference, the anomalous correlation exponent η, which governs $g(\boldsymbol{r}, p_{\rm c}) \propto r^{-d+2-\eta}$, is given by $\eta = 2 + d - \frac{2d}{\tau-1}$.

There is another type of percolation, called *bond percolation*, in which the links of the lattice are occupied (open) with probability p and vacant (closed) with probability $1-p$. In bond percolation, a cluster is defined to be a maximal group of connected bonds. While the percolation thresholds $p_{\rm c}$ on a given lattice in general differ for site and bond percolation, the critical exponents, being universal, do not. Values of $p_{\rm c}$ for site and bond[10] percolation on some common lattices are given in Tab. 2.2.

It is interesting to note[11] that while the critical probability $p_{\rm c}$ for site percolation varies significantly from lattice to lattice, even holding the dimensionality d fixed, when one accounts for the lattice *filling factor* f, defined to be the fraction of the total volume filled when the lattice points are surrounded by hard spheres of maximal radius[12], the product $\phi_{\rm c} \equiv f p_{\rm c}$ is approximately independent of the lattice type and depends only on dimensionality[13], with $\phi_{\rm c}(d=2) \simeq 0.44$ and $\phi_{\rm c}(d=3) \simeq 0.15$. These values also approximately hold for random networks. Thus, if you fill a volume randomly with glass and aluminum marbles, the onset of bulk conduction will occur when the total volume fraction of aluminum exceeds about 15%.

2.1.4 Continuum percolation

Let's now return to our original problem of characterizing the level sets of a smooth random potential $\widetilde{V}(\boldsymbol{r})$. We can associate with this problem a correlated site percolation problem, where the site occupation probability p is given by the fraction of the landscape which lies 'under water', *i.e.* with $\widetilde{V}(\boldsymbol{r}) \le E$, is given by

$$p(E) = \int_{-\infty}^{E} dE'\, \rho(E') \quad . \tag{2.25}$$

As mentioned above, for the continuum percolation problem, the critical energy is $E_{\rm c} = 0$, and therefore $p(0) = p_{\rm c}$. Within the classical continuum percolation picture, the typical cluster size grows as $\xi(E) \propto |E|^{-4/3}$ for $E \approx 0$.

In any physical setting,, the sample dimensions will be finite, and the 2DEG is confined to a

[10] Interesting factoid: $p_{\rm c}^{\rm bond}(d=2) \simeq 2/z$ while $p_{\rm c}^{\rm bond}(d=3) \simeq 3/2z$, where z is the lattice coordination number.
[11] H. Scher and R. Zallen, *J. Chem. Phys.* **53**, 3749 (1970).
[12] *I.e.*, spheres centered on two neighboring lattice sites are tangent.
[13] We stress that the independence of $\phi_{\rm c}$ on lattice structure is not rigorously true, but only approximately so.

d	lattice	z	p_c^{site}	p_c^{bond}
1	chain	2	$1.000\ldots$	$1.000\ldots$
2	honeycomb	3	0.6962	$0.65270\ldots$
2	kagome	4	$0.65260\ldots$	0.5244
2	square	4	0.592746	$0.500\ldots$
2	triangular	6	$0.500\ldots$	$0.34729\ldots$
3	diamond	4	0.43	0.388
3	simple cubic	6	0.3116	0.2488
3	bcc	8	0.246	0.1803
3	fcc	12	0.1998	0.119
4	hypercubic	8	0.197	0.1601
∞	Bethe lattice	z	$1/(z-1)$	$1/(z-1)$

Table 2.2: Site and bond percolation thresholds on various lattices. *Source: Wikipedia (Percolation Threshold)*.

Hall bar of roughly rectangular shape[14]. At the edges of the Hall bar, then, there is a confining potential which rises to some high value. This keeps the electrons from spilling out into the vacuum. The situation is schematically illustrated in Fig. 2.4. When the Fermi energy $E_{\rm F}$ lies in the gap between disorder-broadened Landau levels, there is no percolating network, and currents at the edge of the sample are carried by *edge states* localized along the confining potential region[15]. The percolating network, being infinite in extent in the thermodynamic limit, must connect to the edges. We shall have much more to say about edge states below, but for the moment it is important to apprehend the picture described by Fig. 2.4. Directional edge currents, indicated by the $\odot$ and $\otimes$ symbols in the figure, are responsible for any electrical conduction processes[16].

2.1.5 Scaling of transport data at the IQH transition

The classical picture of the continuum percolation transition is missing something important: quantum tunneling at the saddle points. We know this must be true, but moreover we can

[14]The Hall bar is of course connected to leads for current source and drain, as well as for measuring longitudinal and transverse voltage drops. See Fig. 1.1.

[15]Indeed, this is true whenever $E_{\rm F}$ lies in a *mobility gap*, which is to say whenever $E_{\rm F}$ does not coincide with the continuum percolation threshold. The latter coincidence applies only for energies belonging to a discrete set of values, of measure zero.

[16]At least within linear response theory.

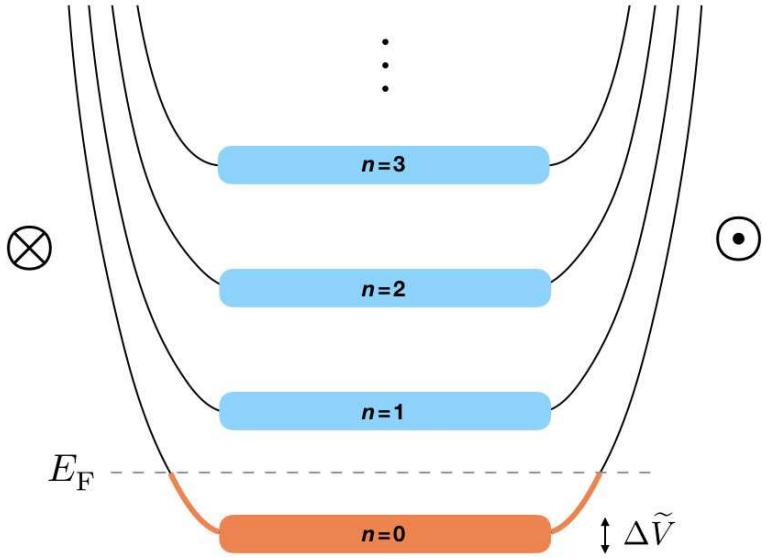

Figure 2.4: Broadened Landau levels and their edge states in a Hall bar. The confining potential forces the energy levels to rise at the edges. When the Fermi level lies between disorder-broadened Landau levels, one or more *edge states* are occupied. The edge states carry the Hall current. The direction of the edge state currents is shown with the $\odot$ and $\otimes$ symbols. Continuum percolation applies when the Fermi energy E_F lies in the vicinity of the center of a disorder-broadened Landau level.

actually *see* it in experiments[17] of the integer quantum Hall (IQH) transition, such as shown in Fig. 2.5. At the lowest temperatures, the Hall conductance/resistance as a function of magnetic field resembles a step function, as B passes through the critical value B_n where $(n+\frac{1}{2})\hbar\omega_c$ passes through the Fermi level. In the vicinity of these critical fields, the correlation length for electrons at the Fermi level diverges as $\xi(B) \propto |B - B_n|^{-\nu}$, where ν is the correlation length exponent. Recall that for classical percolation in $d = 2$ dimensions, $\nu = \frac{4}{3}$ (an exact result). It is then natural to adopt the *scaling hypothesis*

$$\sigma_{yx}(B, L) = \frac{ne^2}{h} + \frac{e^2}{h} F_{\pm}(L/\xi) \tag{2.26}$$

in a system of linear dimension L, where $F_{\pm}(u)$ are scaling functions for $B \gtrless B_n$ with values $F_{\pm}(0) = \frac{1}{2}$ for the transition between consecutive Landau levels[18], $F_{-}(\infty) = 0$ and $F_{+}(\infty) = 1$. The functions $F_{\pm}(u)$ are presumed to interpolate smoothly between their limiting values at $u = 0$ and $u = \infty$. In the thermodynamic limit $L \gg \xi \gg 1$, we have $\sigma_{yx}(B, L \to \infty) = \big(n + \Theta(B - B_n)\big)\, e^2/h$, but with finite L, the step is rounded. Finite temperature T plays a

[17] See, *e.g.*, W. Li *et al.*, *Phys. Rev. Lett.* **102**, 216801 (2009).
[18] This is per spin degree of freedom, or assuming complete spin polarization.

similar role to finite length. With $\beta = 1/k_{\rm B}T$, the scaling *Ansatz* takes the form[19]

$$\sigma_{yx}(B, L, T) = \frac{e^2}{h}\, F(L/\xi, \beta/\xi_\tau) = \frac{e^2}{h}\, \widetilde{F}\big(L^{1/\nu}\,|B - B_n|\,, T^{-1/\nu z}\,|B - B_n|\big) \quad , \tag{2.27}$$

where $\xi_\tau = \xi^z \propto |B - B_n|^{-\nu z}$, where z is the *dynamic critical exponent*. We will see that $z = 1$ for the IQH transition; indeed this can be inferred by comparing transport data as functions of L and of T[20]. The condition $z = 1$ is generally believed to apply in the presence of Coulomb interactions, where the energy scale near criticality is $\hbar\omega \sim e^2/\xi$. For strictly noninteracting and nonrelativistic systems, however, $z = 2$. The reason is that the spectral function $S(\boldsymbol{q}, \omega; E)$ can be expressed using current conservation in terms of the diffusion coefficient $D(\boldsymbol{q}, \omega; E)$ as[21]

$$S(\boldsymbol{q}, \omega; E) = \frac{\hbar\rho(E)}{\pi}\, \frac{q^2 D(\boldsymbol{q}, \omega; E)}{\omega^2 + \big(\boldsymbol{q}^2\, D(\boldsymbol{q}, \omega; E)\big)^2} \quad , \tag{2.28}$$

where $\rho(E)$ is the single particle density of states, with units of $E^{-1}L^{-2}$. If the system is scale invariant at the critical energy $E_{\rm c}$, then $D(\boldsymbol{q}, \omega; E_{\rm c})$ can depend only on the dimensionless combination qL_ω where $L_\omega = \big(\rho(E)\,\hbar\omega\big)^{-1/2}$. Thus if $\rho(E_{\rm c})$ is finite, then $S(\boldsymbol{q}, \omega; E_{\rm c})$ is a function of the combination ω/q^2, which is equivalent to $z = 2$. The takeaway point here is that *interactions must be invoked if the experimentally supported result $z \approx 1$ is to be explained*. We shall return to this point later on below.

Consider now the derivative $d\sigma_{yx}/dB$ as one goes through the IQH transition,

$$\frac{\partial\sigma_{yx}}{\partial B} = \frac{e^2}{h}\, L^{1/\nu}\, \widetilde{F}_u(u, v) + \frac{e^2}{h}\, T^{-1/\nu z}\, \widetilde{F}_v(u, v) \quad , \tag{2.29}$$

where $u \equiv L^{1/\nu}\,|B - B_n|$, $v \equiv T^{-1/\nu z}\,|B - B_n|$, $\widetilde{F}_u = \partial\widetilde{F}/\partial u$, and $\widetilde{F}_v = \partial\widetilde{F}/\partial v$. It is natural to assume that the scaling function $\widetilde{F}(u, v)$ is separately monotonic in each of its arguments, and that the maximum value of $\partial\sigma_{yx}/\partial B$ will occur at $B = B_n$, where $u = v = 0$. Thus,

$$\left(\frac{\partial\sigma_{yx}}{\partial B}\right)_{\rm max} = \frac{e^2}{h}\, \big(c_1\, L^{1/\nu} + c_2\, T^{-1/\nu z}\big) \quad , \tag{2.30}$$

where $c_1 = \widetilde{F}_u(0, 0)$ and $c_2 = \widetilde{F}_v(0, 0)$ are dimensionful constants. In the zero temperature or thermodynamic limits, where we take $T = 0$ or $L = \infty$ at the start, in which case

$$\begin{aligned} \left(\frac{\partial\sigma_{yx}}{\partial B}\right)_{\rm max}(L, 0) &= \frac{e^2}{h}\, d_1\, L^{1/\nu} \\ \left(\frac{\partial\sigma_{yx}}{\partial B}\right)_{\rm max}(\infty, T) &= \frac{e^2}{h}\, d_2\, T^{-1/\nu z} \quad , \end{aligned} \tag{2.31}$$

[19] Here we suppress the $\pm$ indices on the scaling function for notational convenience.

[20] Among the earliest works to report $(d\rho_{xy}/dB)_{\rm max} \sim T^{-\kappa}$ with $\kappa = 1/\nu z = 0.42$ is H. P. Wei *et al.*, *Phys. Rev. Lett.* **61**, 1294 (1988). Samples of different width W were systematically studied by S. Koch *et al.*, *Phys. Rev. Lett.* **67**, 883 (1991), who found that the half-width of the $\rho_{xy}(B, T)$ at the lowest temperatures scaled as $\Delta B \sim W^{-1/\nu}$ with $\nu = 2.34 \pm 0.04$.

[21] See the review by B. Huckestein (RMP, 1995).

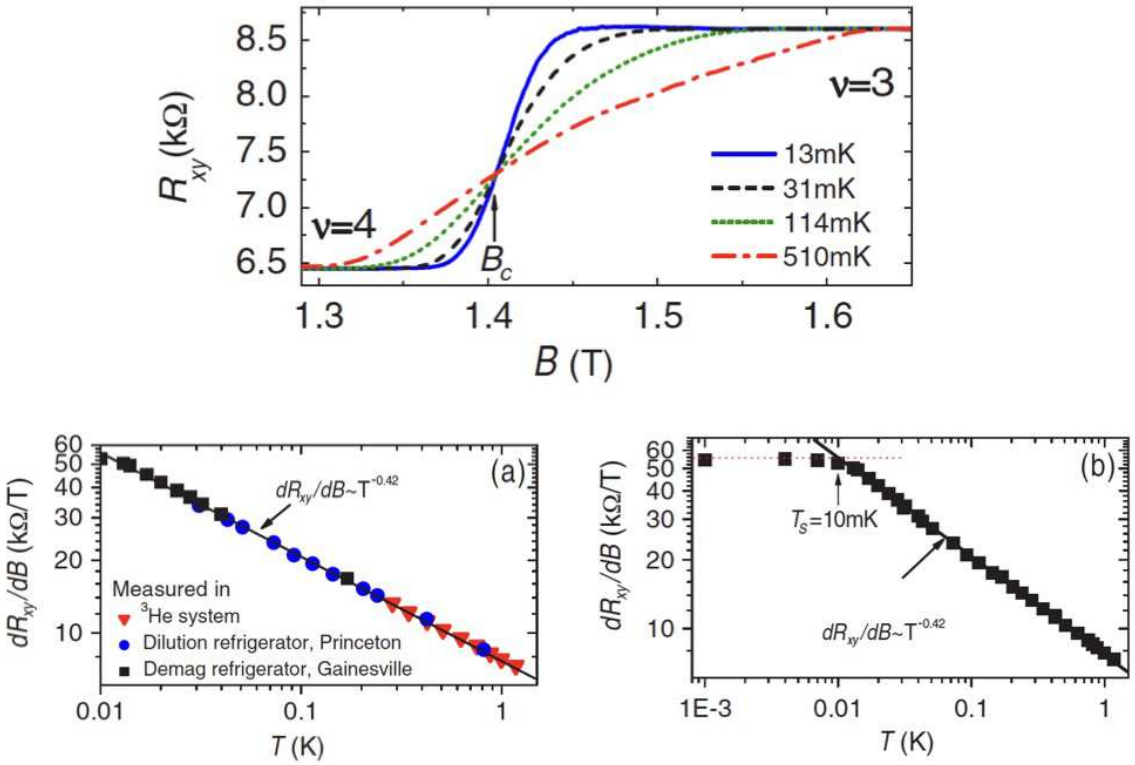

Figure 2.5: Temperature scaling of the $\nu = 3$ to $\nu = 4$ integer quantum Hall transition. Data are from W. Li *et al.*, *Phys. Rev. Lett.* **102**, 216801 (2009). At low temperatures, down to approximately $T = 10\,\mathrm{mK}$, the maximum value of dR_{xy}/dB scales as $T^{0.42} = T^{1/z\nu}$, where $z = 1$ is the dynamical critical exponent and $\nu \approx 2.35$ is the correlation length exponent for the QHE transition.

where $d_1 = \widetilde{F}_u(0,\infty)$ and $d_2 = \widetilde{F}_v(\infty,0)$. Note that while the maximum slope in the $L = \infty$ and $T = 0$ limits is infinite (the derivative of a step function), in each case this infinity is blunted, with the maximum slope being proportional to $L^{1/\nu}$ or $T^{-1/\nu z}$.

In the experiments of Li *et al.*, results of which are shown in Fig. 2.5, the $\nu = 3$ to $\nu = 4$ IQHE transition was observed in transport for temperatures roughly between $T = 1\,\mathrm{mK}$ and $T = 1\,\mathrm{K}$. The sample widths ranged from $W = 100\,\mu\mathrm{m}$ to $W = 500\,\mu\mathrm{m}$. At the critical field $B_\mathrm{c} \approx 1.4\,\mathrm{T}$, the magnetic length is $\ell = 217\,\text{Å}$, so $W/\ell \sim 10^4$. The maximum value of dR_{xy}/dB was found to scale with temperature as $T^{0.42}$ down to $T \approx 10\,\mathrm{mK}$, below which it remained fixed. This latter behavior is associated with finite size effects, *i.e.* the regime $\xi(B) > L$. Over the scaling regime, setting $1/\nu z \simeq 0.42$, one obtains $\nu z \simeq 2.38$. Again, it will turn out that $z = 1$, as can be inferred from size dependence of $(dR_{xy}/dB)_{\max}$, in which case $\nu \simeq 2.38$.

A more general form of the scaling *Ansatz*, for a physical quantity Γ, is

$$\Gamma(B, L, T, \boldsymbol{k}, \omega, \ldots) = \xi^{y_\Gamma}\, F\big(L/\xi, T\xi^{-z}, \boldsymbol{k}\xi, \omega/T, \ldots\big) \tag{2.32}$$

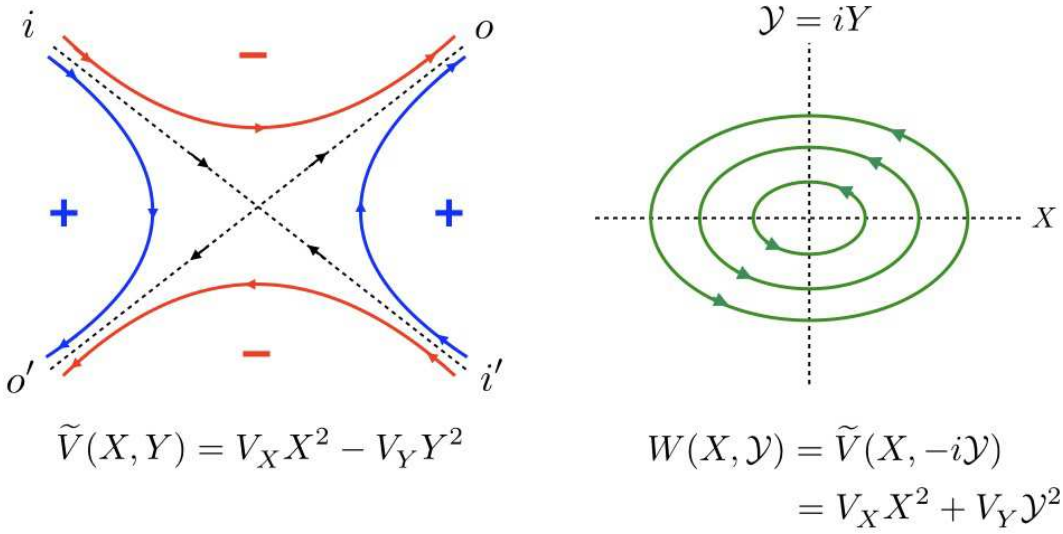

Figure 2.6: Quantum tunneling across saddle points in a random potential $\widetilde{V}(\boldsymbol{r})$. Left: Saddle point in the (X, Y) plane. Right: Upon analytic continuation to imaginary space $\check{Y} = iY$, the saddle becomes a center.

where $\xi \propto |B - B_n|^{-\nu}$ is the correlation length, and where y_Γ is the *scaling dimension* of Γ. The Hall conductivity σ_{xy} has scaling dimension $y = 0$.

A related approach to the temperature scaling is to invoke the notion of an *inelastic scattering length* which diverges as $\ell_{\rm in} \sim T^{-p/2}$ in the limit $T \to 0$. In this picture[22], the scaling variables are ξ/L and $\xi/\ell_{\rm in} \propto \left(T^{-p/2\nu}|B - B_{\rm c}|\right)^{-\nu}$. Thus, in the thermodynamic limit $L \to \infty$, we have $(d\rho_{xy}/dB)_{\rm max} \propto T^{-\kappa}$ with $\kappa = p/2\nu$.

2.1.6 Quantum tunneling across saddle points

Assuming the validity of the scaling *Ansatz*, the transport data are inconsistent with $d = 2$ continuum percolation, for which $\nu = \frac{4}{3}$. What is missing, of course, is quantum mechanics. The problem of tunneling across a saddle point of an electron in a high magnetic field was considered by Fertig and Halperin[23] and by Jain and Kivelson[24]. Consider the situation in the left panel of Fig. 2.6. There are two incoming channels, marked i and i', and two outgoing channels, marked o and o'. The S-matrix acts on incoming flux amplitudes to yield outgoing

[22] See A. M. M. Pruisken, *Phys. Rev. Lett.* **61**, 1297 (1988).
[23] H. A. Fertig and B. I. Halperin, *Phys. Rev. B* **36**, 7969 (1987).
[24] J. K. Jain and S. Kivelson, *Phys. Rev. B* **37**, 4111 (1988).

flux amplitudes, *viz.*

$$\begin{pmatrix} o' \\ o \end{pmatrix} = \overbrace{\begin{pmatrix} r & t' \\ t & r' \end{pmatrix}}^{\mathcal{S}} \begin{pmatrix} i \\ i' \end{pmatrix} \quad , \tag{2.33}$$

where r, r' are reflection amplitudes and t, t' are transmission amplitudes. The reflection and transmission *probabilities* are given by the squares of the corresponding amplitudes,

$$R = |r|^2 \quad , \quad T = |t|^2 \quad , \quad R' = |r'|^2 \quad , \quad T' = |t'|^2 \quad . \tag{2.34}$$

Unitarity of $\mathcal{S}$ guarantees that $R' = R$ and $T' = T$, as well as $R + T = 1$. Note that $\mathcal{S} \in \mathsf{U}(2)$, which has dimension four. This allows us to write $t' = t^* \exp(-i\delta)$ and $r' = -r^* \exp(-i\delta)$ with $r = \sin(\theta)\exp(i\psi)$ and $t = \cos(\theta)\exp(i\omega)$. The four parameters are then $(\theta, \psi, \omega, \delta)$.

It is important to recognize that the complex scalars $\{i, i', o, o'\}$ are *flux amplitudes* and not wavefunction amplitudes. Unitarity of $\mathcal{S}$ means that

$$|o'|^2 + |o|^2 = |i|^2 + |i'|^2 \quad , \tag{2.35}$$

and is a statement about *current conservation*. A simple illustration of the difference is afforded by consideration of the one-dimensional step potential $V(x) = V_0\,\Theta(x)$. We write

$$\begin{aligned} x < 0 \ : \quad & \psi(x) = I\,e^{ikx} + O'\,e^{-ikx} \\ x > 0 \ : \quad & \psi(x) = O\,e^{ik'x} + I'\,e^{-ik'x} \quad , \end{aligned} \tag{2.36}$$

where the energy

$$E = \frac{\hbar^2 k^2}{2m} = \frac{\hbar^2 k'^2}{2m} + V_0 \tag{2.37}$$

is conserved in by the scattering process, and is assumed to be positive. The requirements that $\psi(x)$ and $\psi'(x)$ be continuous at $k = 0$ provide two conditions on the four wavefunction amplitudes:

$$\begin{aligned} I + O' &= O + I' \\ k\,(I - O') &= k'\,(O - I') \quad . \end{aligned} \tag{2.38}$$

The flux amplitudes $\{i, i', o, o\}$ are related to the wavefunction amplitudes $\{I, I', O, O'\}$ by a multiplicative factor of the square root of the velocity, where $v = \hbar k/m$ and $v' = \hbar k'/m$:

$$\begin{pmatrix} i \\ o' \end{pmatrix} = \sqrt{v} \begin{pmatrix} I \\ O' \end{pmatrix} \qquad , \qquad \begin{pmatrix} o \\ i' \end{pmatrix} = \sqrt{v'} \begin{pmatrix} O \\ I' \end{pmatrix} \quad . \tag{2.39}$$

One may now derive the $\mathcal{S}$-matrix,

$$\mathcal{S} = \begin{pmatrix} r & t' \\ t & r' \end{pmatrix} = \frac{1}{1+\eta} \begin{pmatrix} 1-\eta & 2\sqrt{\eta} \\ 2\sqrt{\eta} & \eta - 1 \end{pmatrix} \quad , \tag{2.40}$$

where

$$\eta = \frac{v'}{v} = \frac{k'}{k} = \sqrt{1 - \frac{V_0}{E}} \quad . \tag{2.41}$$

One can check that $\mathcal{S}^\dagger \mathcal{S} = 1$. However note that the matrix $\widetilde{\mathcal{S}}$ which acts on the wavefunction amplitudes, with

$$\begin{pmatrix} O' \\ O \end{pmatrix} = \widetilde{\mathcal{S}} \begin{pmatrix} I \\ I' \end{pmatrix} \tag{2.42}$$

is related to $\mathcal{S}$ by

$$\widetilde{\mathcal{S}} = \begin{pmatrix} 1/\sqrt{v'} & 0 \\ 0 & 1/\sqrt{v} \end{pmatrix} \mathcal{S} \begin{pmatrix} \sqrt{v} & 0 \\ 0 & \sqrt{v'} \end{pmatrix} \tag{2.43}$$

and is in general not unitary. Note also that when $v = v'$ we have $\widetilde{\mathcal{S}} = \mathcal{S}$.

Saddle point transmission probability

For an electron in the potential

$$V(x, y) = V_x \, x^2 - V_y \, y^2 \quad , \tag{2.44}$$

Fertig and Halperin (1987) obtained the transmission probability[25]

$$T(\epsilon) = \frac{1}{1 + \exp(\pi\epsilon)} \quad , \tag{2.45}$$

where $\epsilon = \big(E - (n + \frac{1}{2})\hbar\omega_{\rm c}\big)/\Gamma$ and $\Gamma \approx \ell^2 (V_x V_y)^{1/2}$, assuming $\ell^2 \, V_{x,y} \ll \hbar\omega_{\rm c}$. Note that for $|\epsilon| \gg 1$ one has

$$T(\epsilon) \simeq \begin{cases} \exp\big(-\pi|\epsilon|\big) & \text{if } \epsilon > 0 \\ 1 - \exp\big(-\pi|\epsilon|\big) & \text{if } \epsilon < 0 \end{cases} \quad . \tag{2.46}$$

Similarly,

$$R(\epsilon) = 1 - T(\epsilon) \simeq \begin{cases} 1 - \exp\big(-\pi|\epsilon|\big) & \text{if } \epsilon > 0 \\ \exp\big(-\pi|\epsilon|\big) & \text{if } \epsilon < 0 \end{cases} \quad . \tag{2.47}$$

This conforms to the situation in Fig. 2.6: If $\epsilon \gg 1$, the transmission is almost purely from i to o' and from i' to o, corresponding to $R \approx 1$ and $T \approx 0$. If on the other hand $\epsilon \ll -1$, then the transmission is almost purely from i to o and from i' to o', hence $R \approx 0$ and $T \approx 1$.

[25] For us, the parameter ϵ is the negative of that in Fertig and Halperin.

Instantons and tunnel splittings

Following Jain and Kivelson (1988), we can also apply the coherent state path integral to this problem. The partition function at inverse temperature $\beta = 1/k_{\rm B}T$ is given by

$$Z(\beta) = \mathsf{Tr}\, e^{-\beta H} = \int \frac{d^2R}{2\pi\ell^2}\, \langle\, \boldsymbol{R}\,|\, e^{-\beta H}\,|\,\boldsymbol{R}\,\rangle = \int\limits_{\boldsymbol{R}(0)=\boldsymbol{R}(\hbar\beta)} D\big[R(\tau),\bar{R}(\tau)\big]\; e^{-\mathcal{S}_{\rm E}/\hbar} \quad . \tag{2.48}$$

The partition function is the Laplace transform of the density of states, and as such incorporates all information about the energy spectrum, including tunnel splittings. We measure energies with respect to $(n+\frac{1}{2})\hbar\omega_{\rm c}$, in which case

$$\mathcal{S}_{\rm E}\big[X(\tau),Y(\tau)\big] = \int\limits_0^{\hbar\beta} d\tau\, \left[\frac{i\hbar}{2\ell^2}\big(Y\dot{X} - X\dot{Y}\big) + \widetilde{V}(X,Y)\right] + \Delta\mathcal{S}_{\rm E} \quad , \tag{2.49}$$

where $\widetilde{V}(X,Y) \equiv \widetilde{V}(R|\bar{R}) = \langle\, \boldsymbol{R}\,|\,V\,|\,\boldsymbol{R}\,\rangle$ with $R = X + iY$ and $\bar{R} = X - iY$, and where $\Delta\mathcal{S}_{\rm E}$ is the boundary discontinuity term. The equations of motion obtained by extremizing $\mathcal{S}_{\rm E}$ force us to analytically continue to imaginary *space*. In terms of the complexified guiding center coordinates R and $\bar{R}$, this entails $\bar{R} \neq R^*$ along the instanton path. Writing $\mathcal{Y} \equiv iY$[26] and defining $W(X,\mathcal{Y}) \equiv \widetilde{V}(X,-i\mathcal{Y})$, we obtain $\mathcal{S}_{\rm E} = \int_0^{\hbar\beta} d\tau\; L(X,\mathcal{Y},\dot{X},\dot{\mathcal{Y}}) + \Delta\mathcal{S}_{\rm E}$, where the Lagrangian is

$$L = \frac{\hbar}{2\ell^2}\big(\mathcal{Y}\dot{X} - X\dot{\mathcal{Y}}\big) + W(X,\mathcal{Y}) \quad . \tag{2.50}$$

The equations of motion are then

$$\dot{X} = -\frac{\ell^2}{\hbar}\,\frac{\partial W}{\partial \mathcal{Y}} \qquad , \qquad \dot{\mathcal{Y}} = \frac{\ell^2}{\hbar}\,\frac{\partial W}{\partial X} \quad . \tag{2.51}$$

Note that W is then conserved along the trajectory, since

$$\frac{d}{dt}\,W\big(X(t),\mathcal{Y}(t)\big) = \frac{\partial W}{\partial X}\,\dot{X} + \frac{\partial W}{\partial \mathcal{Y}}\,\dot{\mathcal{Y}} = 0 \quad . \tag{2.52}$$

Assuming the boundary discontinuity term vanishes, the Euclidean action is then

$$\mathcal{S}_{\rm E} = \beta E + \frac{A}{\ell^2} \tag{2.53}$$

where E is the conserved value of the potential along the instanton trajectory and A is the area enclosed by the trajectory. For the saddle point potential $\widetilde{V}(X,Y) = V_X X^2 - V_Y Y^2$, we have $W(X,\mathcal{Y}) = V_X X^2 + V_Y \mathcal{Y}^2$, and setting $W = E$ we obtain the ellipse

$$\frac{X^2}{a^2} + \frac{\mathcal{Y}^2}{b^2} = 1 \quad , \tag{2.54}$$

[26] Note we have repurposed the symbol $\mathcal{Y}$ here.

with $a = (E/V_X)^{1/2}$ and $b = (E/V_Y)^{1/2}$. The full area of the ellipse is $A = \pi ab = \pi E/(V_X V_Y)^{1/2}$, hence $A/\ell^2 = \pi\epsilon$, where $\epsilon = E/\Gamma$. Recall that here we measure E relative to the center of the Landau level at $E_n = (n + \frac{1}{2})\hbar\omega_c$.

For weak tunneling, the amplitude t is proportional to the single instanton contribution after subtracting off the βE term, and is given by $t = \exp(-A/2\ell^2)$ since only half of the elliptical trajectory of $(X, \mathcal{Y})$ is traversed in crossing the saddle. The transmission coefficient is then given by $T = |t|^2 = \exp(-A/\ell^2) = \exp(-\pi\epsilon)$, exactly as in Fertig and Halperin. For smaller values of ϵ, multiple instanton paths must be summed over in order to get the Fertig-Halperin result $T(\epsilon) = \big[1 + \exp(\pi\epsilon)\big]^{-1}$.

Mil'nikov-Sokolov argument

G. Mil'nikov and I. Sokolov (1988) published a seductive argument[27] purporting to establish that the correlation length exponent for quantum continuum percolation should be given by $\nu_{QU} = \nu_{CL} + 1 = \frac{7}{3}$. Consider a distance $r \gg \xi_{CL}(E)$, over which one expects to encounter $\sim r/\xi_{CL}(E)$ such saddles. The probability of transmission across this entire distance is then

$$T_{QU}(E) \sim \big(T_{saddle}(E)\big)^{r/\xi_{CL}(E)} = e^{-\pi r|E|/\Gamma\xi_{CL}(E)} \equiv e^{-r/\xi_{QU}(E)} \quad . \tag{2.55}$$

Thus, we expect

$$\xi_{QU}(E) = \langle\Gamma\rangle \frac{\xi_{CL}(E)}{\pi|E|} \propto |E|^{-7/3} \quad , \tag{2.56}$$

where $\langle\Gamma\rangle$ is an average over the Γ parameter over many saddles. As we shall see, this result is quite close to the experimentally determined value of $\nu = 2.35$ (see Fig. 2.5). It is also close to the earliest numerical simulation values of ν_{QU} for the IQH transition. Alas, the Mil'nikov-Sokolov argument is bogus – at least insofar as it purports to describe the critical properties of the disordered noninteracting 2DEG in the LLL – because it doesn't properly account for the connectivity of the saddle point network, treating it instead as a chain with no closed loops. It also doesn't account for quantum interference effects associated with backscattering from saddle points. Below we shall see how a more sophisticated treatment, the Chalker-Coddington *network model of quantum percolation*, can properly model the critical behavior of noninteracting electrons in a magnetic field and a random potential.

Away from the quantum critical point near the center of the Landau level – but not too far away – the Mil'nikov-Sokolov picture should be applicable[28]. In this regime, the quantum tunneling probability $e^{-\pi|E|/\Gamma} \ll 1$ is weak, and we can consider only transmission across each saddle, with no closed loops associated with reflection paths. Recall $\Gamma = \ell^2 (V_x V_y)^{1/2} \propto W\ell^2/d^2$,

[27] G. V. Mil'nikov and I. M. Sokolov, *Pis'ma Zh. Eksp. Teor. Fiz.* **48**, 494 (1988) [*JETP Lett.* **48**, 536 (1988)].

[28] See M. M. Fogler, A. Y. Dobin, and B. I. Shklovskii, *Phys. Rev. B* **57**, 4614 (1998). I thank my colleague Misha Fogler for explaining this to me.

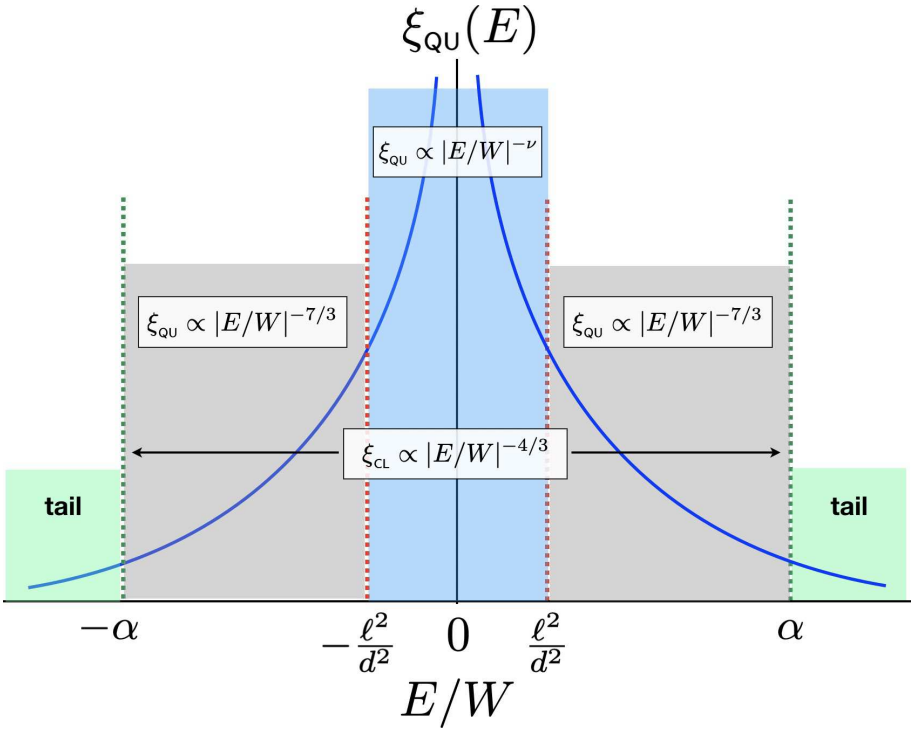

Figure 2.7: Regimes of behavior for $\xi_{CL}(E)$ and $\xi_{QU}(E)$ in a smooth random potential $V(\boldsymbol{r})$ whose RMS fluctuations are W and whose correlation length is d. Blue: Critical regime, in which the exponent ν for quantum percolation is obtained from network model simulations. Gray: Mil'nikov-Sokolov regime, in which quantum tunneling across saddle points is weak but the classical percolation is still in the critical regime. Green: Tail regime, in which the physics is dominated by local fluctuations of $V(\boldsymbol{r})$.

where W is the RMS potential fluctuation and d the correlation length of the potential, assuming there is a single length scale associated with $V(\boldsymbol{r})$, which is the case if $V(\boldsymbol{r})$ is chosen according to the distribution functional

$$P\big[V(\boldsymbol{r})\big] = P[0]\exp\left\{-\frac{1}{2W^2d^2}\int d^2r\,\Big[V^2 + d^2(\boldsymbol{\nabla}V)^2\Big]\right\} \quad . \tag{2.57}$$

Classical continuum percolation then says $\xi_{CL}(E) = Cd\,|E/W|^{-4/3}$, where C is a dimensionless constant. This form is valid provided $|E/W|$ is sufficiently small, which is to say within the critical regime, which is to say $|E| < \alpha W$, where $\alpha = \mathcal{O}(1)$ is a dimensionless constant. The condition that reflections may be neglected is tantamount to $|E| \gtrsim \Gamma$, and thus the range over which we expect the MS argument to be valid is

$$(\ell/d)^2 \lesssim |E|/W \lesssim \alpha \quad . \tag{2.58}$$

For potentials which are very smooth on the scale of ℓ, this criterion is easily satisfied. In this regime, we therefore expect $\xi_{QU}(E) \propto |E|^{-7/3}$. As we shall see, this exponent is quite close to

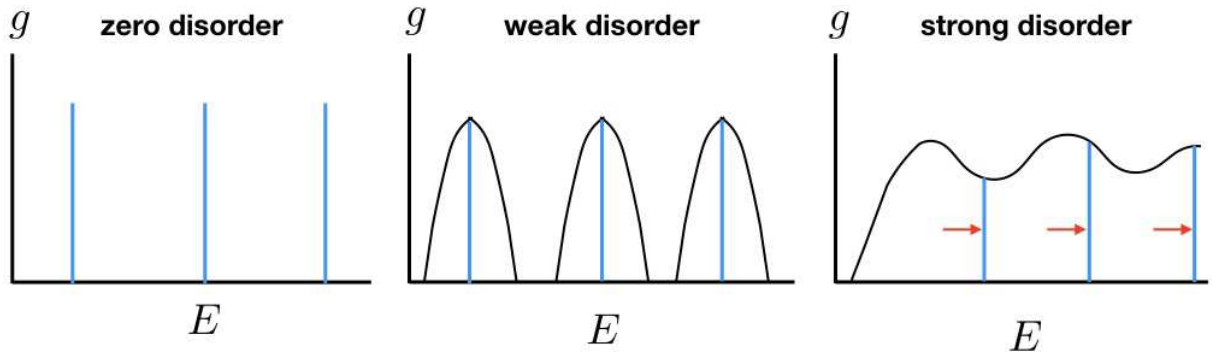

Figure 2.8: Floating up of extended states in the presence of disorder.

what is observed in scaling analyses of experiments, but is inconsistent with the most recent best results for the correlation length exponent for quantum percolation networks.

2.1.7 Landau level mixing and "floating" of extended states

At high fields, each Landau level carries one unit of Hall conductivity e^2/h, *i.e.* the $n^{\rm th}$ Landau level carries Chern number $\Delta C_n = 1$ (or $\Delta C_n = -1$ as in our case with $\boldsymbol{B} = -B\hat{\boldsymbol{z}}$). If we ignore Landau level mixing, this state of affairs persists to weak fields as well, since each LL remains independent. However, in the $B = 0$ limit, in a two-dimensional disordered system with no interactions, all electronic states are known to be localized and the system is an integer. As $B \to 0$, the cyclotron gap between LLs becomes smaller, tending to zero, and eventually we know LL mixing must apply. What happens to all the extended states lying at the LL centers[29]? An early view suggested that extended states must *float up* in energy as $B \to 0$ in the presence of disorder. A cartoon of this notional state of affairs is depicted in Fig. 2.9(a). According to this picture, one should expect reentrant behavior in $\sigma_{xy}(n, B)$ as a function of B at fixed density n. Note how in this picture, there are direct transitions only between states with $\Delta C = \pm 1$, and none for $|\Delta C| > 1$.

What actually occurs, both in numerical simulations as well as in experiments, appears to be more complicated and as yet not fully understood. The fate of extended states at weak disorder was investigated numerically by Sheng, Weng, and Wen (SWW), using a tight binding model for spin-polarized electrons.

$$H = -\sum_{\langle \boldsymbol{r}\boldsymbol{r}'\rangle} \left(e^{iA_{\boldsymbol{r}\boldsymbol{r}'}}\, c^\dagger_{\boldsymbol{r}}\, c_{\boldsymbol{r}'} + e^{-iA_{\boldsymbol{r}\boldsymbol{r}'}}\, c^\dagger_{\boldsymbol{r}'}\, c_{\boldsymbol{r}} \right) + \sum_{\boldsymbol{r}} W_{\boldsymbol{r}}\, c^\dagger_{\boldsymbol{r}}\, c_{\boldsymbol{r}} \quad , \tag{2.59}$$

where the flux per plaquette is taken to be $\phi = 2\pi p/q$ local disorder potential at lattice site $\boldsymbol{r}$ is

[29] Due to asymmetry in the distribution of $\widetilde{V}(\boldsymbol{r})$ and LL mixing, the extended states are not obliged to lie exactly at $E_n = (n + \frac{1}{2})\hbar\omega_{\rm c}$.

given by

$$W_{\boldsymbol{r}} = \frac{W}{\pi} \sum_{\boldsymbol{r}'} f_{\boldsymbol{r}'}\, e^{-|\boldsymbol{r}-\boldsymbol{r}'|^2/\lambda^2} \quad , \tag{2.60}$$

where on each site $f_{\boldsymbol{r}}$ is uniformly distributed on the interval $[-1, 1]$. Thus W and λ are the strength and correlation length of the random disorder. SWW's results are summarized in Fig. 2.9(b). The maximum lattice size was 32×64. The transition to the insulating state occurs along the dark black curve, thus direct transitions were observed from each of $C = 1, 2, 3, 4$ to $C = 0$.

Experiments by Kravchenko *et al.* in Si MOSFETS, shown in Fig. 2.9(c,d), show an apparent violation of the $|\Delta C| = 1$ rule for the IQH transitions inferred from the cartoon picture. Rather, there are a sequence of direct transitions from IQH states with $C = 1$, $C = 2$, $C = 4$, and $C = 6$ to a state they identify as an "insulator". Note how the $C = 3$ and $C = 5$ states get crowded out as disorder increases but before one reaches the $C = 0$ insulator. Thus, there are direct transitions observed between $C = 2$ and $C = 4$ and between $C = 4$ and $C = 6$. These $|\Delta C| = 2$ transitions may be associated with spin-orbit effects in the presence of interactions, although this is more likely to pertain in GaAs heterojunctions where the spin-orbit interaction is stronger than in Si due to larger nuclear Z.

However, there is a rather severe problem with Kravchenko *et al.*'s interpretation of their "insulator"[30]. Consider their results for the electron scattering rate τ^{-1}, which they extract from the $B = 0$ expression for the mobility $\mu = e\tau/m^*$. Using $m^* = (m_{\rm t}^2\, m_{\rm l})^{1/3} = 0.22\, m_{\rm c}$ for the conduction electrons in Si[31], if we divide the Drude formula for ρ_{xx} by the quantum of resistance h/e^2, we obtain

$$\frac{e^2}{h}\,\rho_{xx} = \frac{m^*}{2\pi n\hbar\tau} = \overbrace{\frac{0.22\, m_{\rm e} \times 10^{14}\,{\rm s}^{-1}}{2\pi \times 1.055 \times 10^{-27}\,{\rm erg}\cdot{\rm s} \times 10^{11}\,{\rm cm}^{-2}}}^{=\,3.32} \times \frac{\tau^{-1}\big[10^{14}\,{\rm s}^{-1}\big]}{n\big[10^{11}\,{\rm cm}^{-2}\big]} \quad . \tag{2.61}$$

Thus, for $n \approx 10^{11}\,{\rm cm}^{-1}$ and $\tau^{-1} \lesssim 10^{14}\,{\rm s}^{-1}$, $\rho_{xx} \sim h/e^2$, which can hardly be identified with an insulator! This state is best identified as a correlated metal.

2.2 Integer Quantum Hall Transition

2.2.1 Introduction

Recall the eigenfunctions in the Landau strip basis discussed in §1.3.5. The geometry is cylindrical, with $x \in \mathbb{R}$ and $y \in [0, L_y]$ with periodic boundary conditions in the y-direction. Choos-

[30] I am grateful to Steven Kivelson for explaining this to me.

[31] $m_{\rm t}^* = 0.082\, m_{\rm e}$ and $m_{\rm l}^* = 1.64\, m_{\rm e}$ are the transverse and longitudinal effective masses for Si conduction electrons.

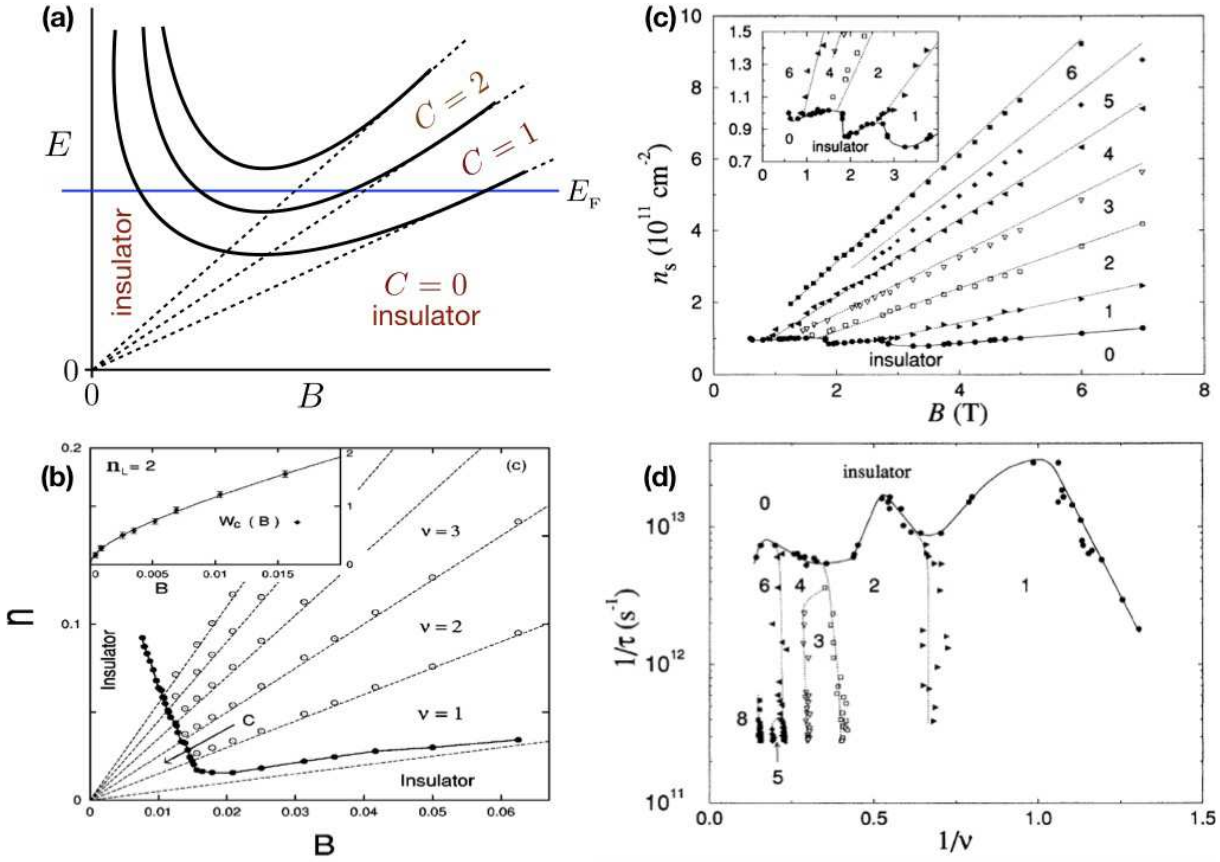

Figure 2.9: Extended and localized states in the quantum Hall effect (a) Early cartoon picture, which suggests reentrant behavior as B is varied at fixed density. Dashed lines correspond to $E = E_n = (n + \frac{1}{2})\hbar\omega_c$. (b) Numerical data of D. N. Sheng, Z. Y. Weng, and X. G. Wen, *Phys. Rev. B* **64**, 165317 (2001). (c) and (d) Experimental data in Si MOSFETS, from S. V. Kravchenko *et al.*, *Phys. Rev. Lett.* **75**, 910 (1995). The scattering rate $1/\tau$ extracted from the data serves as a measure of the strength of the disorder potential $\widetilde{V}(\boldsymbol{r})$. The state labeled as "insulator" in panels (c) and (d) is in fact a correlated metal.

ing the gauge $\boldsymbol{A} = A_y\,\hat{\boldsymbol{y}}$ with $A_y = -Bx$, we obtained the eigenfunctions

$$\psi_{n,j}(x,y) = L_y^{-1/2}\, e^{ik_y\, y}\, \phi_n(x - \ell^2 k_y) \quad , \tag{2.62}$$

where $E_{n,j} = (n+\frac{1}{2})\hbar\omega_c$ and where $\phi_n(x) = (2^n n!)^{-1/2}(\pi\ell^2)^{-1/4}\mathsf{H}_n(x/\ell)\,\exp(-x^2/2\ell^2)$. Note that $k_y = 2\pi j/L_y$ is quantized according to the PBC $\exp(ik_yL_y) = 1$.

Now consider the gauge $A_y = -Bx + \alpha\phi_0/L_y$ where $\phi_0 = hc/e$ is the Dirac flux quantum and where $\alpha \in \mathbb{R}$ is a dimensionless free parameter. We still have $\boldsymbol{\nabla}\times\boldsymbol{A} = -B\hat{\boldsymbol{z}}$, and it is easy to check that this incorporates the gauge transformation

$$H_0(\alpha) = e^{-2\pi i\alpha y/L_y}\, H_0(0)\, e^{+2\pi i\alpha y/L_y} \quad . \tag{2.63}$$

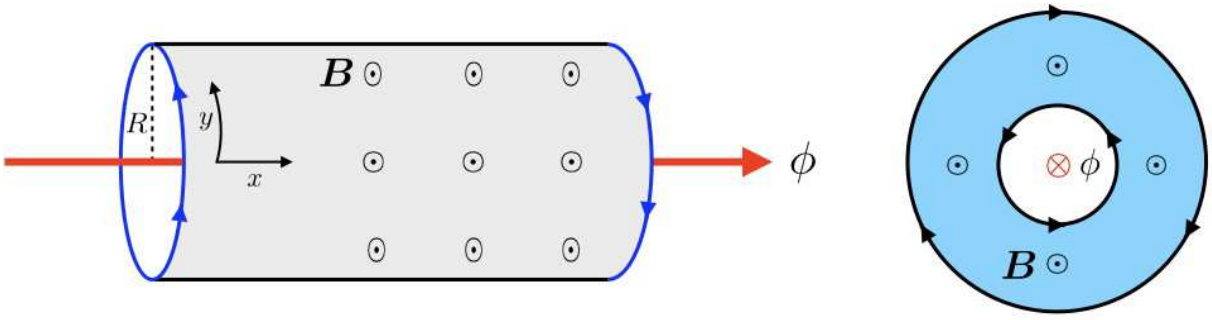

Figure 2.10: Cylindrical and Corbino ring geometries. With each additional fluxoid $\Delta\phi = hc/e$ threaded, an integer number of electrons are transferred from one edge to the other.

One might think that this permits us to write $\psi_{n,j}(x,y;\alpha) = \exp(-2\pi i\alpha y/L_y)\,\psi_{n,j}(x,y;0)$, however such a wavefunction does not satisfy the PBCs except in cases where $\alpha \in \mathbb{Z}$. The resolution is to first shift the k_y quantization such that $\exp(ik_yL_y)\,\exp(-2\pi i\alpha) = 1$, *i.e.* $k_y = 2\pi(j+\alpha)/L_y$. Then

$$\psi_{n,j}(x,y;\alpha) = L_y^{-1/2}\,\exp(2\pi ijy/L_y)\,\phi_n\left(x - \frac{2\pi(j+\alpha)\ell^2}{L_y}\right) \quad , \tag{2.64}$$

Note that

$$\psi_{n,j}(x,y;\alpha+1) = e^{-2\pi iy/L_y}\,\phi_{n,j+1}(x,y;\alpha) \quad , \tag{2.65}$$

which is an allowed transformation, *i.e.* one which preserves the boundary conditions. What has happened (see Fig. 2.10 is that we have threaded our cylinder with α Dirac flux quanta. As we adiabatically increase the flux parameter α by $\Delta\alpha = 1$, the $j^{\rm th}$ Landau strip eigenfunction evolves into the $(j+1)^{\rm th}$ eigenfunction, up to the PBC-preserving gauge factor, $\exp(-2\pi iy/L_y)$.

Now imagine that there is also potential $V_{\rm conf}(x)$ which confines the system in the x-direction. So long as $|\ell\,\nabla V_{\rm conf}| \ll \hbar\omega_{\rm c}$, the eigenfunctions will remain localized along the Landau strips, and the energy eigenvalues will be given by $E_{n,j} = V_{\rm conf}(x_{j,\alpha})$, where $x_{j,\alpha} = 2\pi(j+\alpha)\ell^2/L_y$. If the chemical potentials on the two edges differ by $\Delta\mu = -eV$, where V is the voltage drop, then the current may be computed as

$$I = -c\,\frac{\partial U}{\partial\phi} \approx -c\,\frac{\Delta U}{\phi_0} = c\,\frac{neV}{hc/e} = \frac{ne^2}{h}\,V \quad , \tag{2.66}$$

where U is the total energy, and where n is the number of edge state channels on each side lying below the Fermi level (see Fig. 2.4). This is Laughlin's argument[32] for the quantization of Hall conductance: $\sigma_{yx} = I/V = ne^2/h$. Furthermore, even if the potential $V(\boldsymbol{r})$ is nonzero in the bulk, provided the edge states are localized along the walls of the confining potential, adiabatic increase of the dimensionless flux parameter α by $\Delta\alpha = 1$ still must result in the shifting of edge states by $\Delta j = 1$ for each fully occupied Landau level, and must therefore result in an integer contribution to σ_{yx} in units of e^2/h. The adiabatic change of the threaded

[32] R. B. Laughlin, *Phys. Rev. Lett.* **23**, 5632 (1981).

flux $\Delta\phi = \phi_0$ in the cylindrical or Corbino geometries acts as a pump, transferring n electrons from one side of the sample to the other. Laughlin's argument was subsequently sharpened by Halperin[33].

2.2.2 Replica field theory of the IQH transition

A replica field theory of the transition was proposed in 1983 by Khmel'nitskii[34] and by Libby, Levine, and Pruisken[35], based on the Lagrangian,

$$\mathcal{L}(Q) = \tfrac{1}{4}\,\tilde\sigma^0_{xx}\,\mathsf{Tr}\,(\partial_\mu Q)^2 + \tfrac{1}{8}\,\tilde\sigma^0_{xy}\,\mathsf{Tr}\,\big(\epsilon^{\mu\nu} Q\,\partial_\mu Q\,\partial_\nu Q\big) \quad , \tag{2.67}$$

where $\tilde\sigma^0_{\mu\nu} = h\sigma^0_{\mu\nu}/e^2$ is the dimensionless bare conductivity tensor (*i.e.* at some microscopic length scale), and where $Q(x,y)$ lives in the symmetric coset space $\mathsf{U}(2n)/\mathsf{U}(n)\times\mathsf{U}(n)$ in the $n\to 0$ replica limit. The second term is a topological invariant:

$$\int d^2x\;\mathsf{Tr}\,\big(\epsilon^{\mu\nu} Q\,\partial_\mu Q\,\partial_\nu Q\big) = 16\pi i q \quad , \tag{2.68}$$

where $q\in\mathbb{Z}$; this is true for all n. This field theory is difficult to analyze due to the topological term, but a dilute instanton gas expansion generates the renormalization group flow[36]

$$\begin{aligned}\frac{\partial\tilde\sigma_{xx}}{\partial\ln L} &= -\frac{1}{2\pi^2\tilde\sigma_{xx}} - c\,\tilde\sigma_{xx}\,e^{-2\pi\tilde\sigma_{xx}}\cos(2\pi\tilde\sigma_{xy}) \\ \frac{\partial\tilde\sigma_{xy}}{\partial\ln L} &= -c\,\tilde\sigma_{xx}\,e^{-2\pi\tilde\sigma_{xx}}\sin(2\pi\tilde\sigma_{xy}) \quad .\end{aligned} \tag{2.69}$$

These results are purported to hold at weak coupling $g = 2/\tilde\sigma^0_{xx} \ll 1$. Note that the exponential terms are *nonperturbative* and proportional to $\exp(-4\pi/g)$. What happens for strong coupling as $g\to 0$? We can only guess, consistent with symmetry and physical intuition, and a sketch is shown in Fig. 2.11. The flow in Eqns. 2.69 is valid for large σ^0_{xx}. We know that $\sigma_{xy} = pe^2/h$ must be a stable RG fixed point for $p\in\mathbb{Z}$. This naturally leads to a conjectured unstable fixed point, depicted in red in the figure, and the associated flow lines. We emphasize that the Lagrangian density $\mathcal{L}(Q)$ corresponds to a *two-dimensional* field theory for *noninteracting* electrons.

2.2.3 Chalker-Coddington network model

Despite the elegance of Laughlin's argument and the proposed nonlinear sigma model field-theoretic formulation of the IQH transitions, detailed investigations of the transition, *e.g.* in

[33] B. I. Halperin, *Phys. Rev. B* **25**, 2185 (1982).
[34] D. E. Khmel'nitskii, *Pis'ma Zh. Eksp. Teor. Fiz.* **38**, 454 (1983) [*JETP Lett.* **38**, 552 (1984)].
[35] H. Levine, S. B. Libby, and A. M. M. Pruisken, *Phys. Rev. Lett.* **51**, 1915 (1983).
[36] A. M. M. Pruisken, in *The Quantum Hall Effect*, R. Prange and S. M. Girvin, eds. (Springer, 1987).

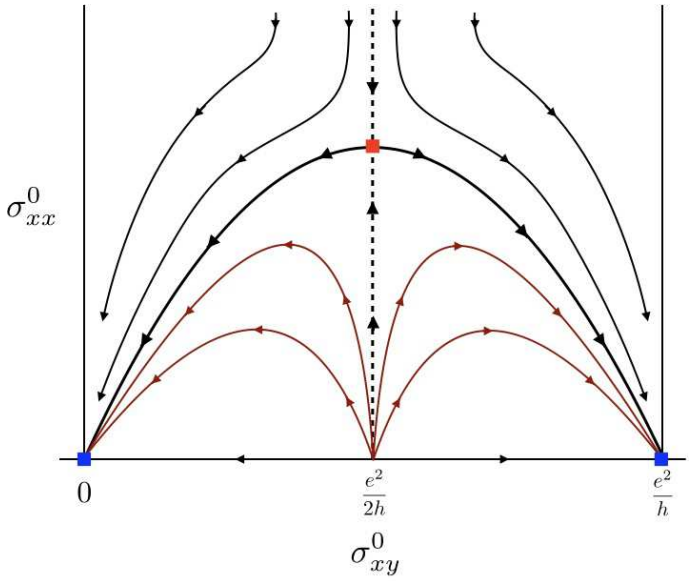

Figure 2.11: Khmel'nitskii-Pruisken RG flow for the nonlinear sigma model field theory of the integer quantum Hall effect. The flow is periodic in σ^0_{xy} with period h/e^2. The conjectured flow at strong coupling is shown in brown. The blue squares represent stable RG fixed points, and the red square an unstable RG fixed point.

terms of critical behavior, is largely problem for numerical simulators. One can, for example, model the an electron in a random potential in a magnetic field with a tight binding model. Such approaches are not optimally suited to gleaning the essential critical behavior because they retain a lot of inessential details, such as regions with high peaks and regions with low valleys, which slow down the computation. A much more efficient model was devised by Chalker and Coddington in 1988[37], who realized that the most important physics is that associated with tunneling across saddle points.

We begin with the single saddle point of Figs. 2.6. The incoming flux amplitudes i and i' scatter into the outgoing amplitudes o and o' according to the linear relation of Eqn. 2.33. As shown in Fig. 2.13, this linear relation between incoming and outgoing amplitudes may be recast, reading the scattering diagram from left to right, as a relation between "left" and "right" amplitudes. Specifically,

$$\begin{pmatrix} o' \\ o \end{pmatrix} = \overbrace{\begin{pmatrix} r & t^* e^{-i\delta} \\ t & -r^* e^{-i\delta} \end{pmatrix}}^{\mathcal{S}} \begin{pmatrix} i \\ i' \end{pmatrix} \qquad \Longrightarrow \qquad \begin{pmatrix} o \\ i' \end{pmatrix} = \overbrace{\begin{pmatrix} 1/t^* & -r^*/t^* \\ -r\, e^{i\delta}/t^* & e^{i\delta}/t^* \end{pmatrix}}^{\mathcal{M}} \begin{pmatrix} i \\ o' \end{pmatrix} . \tag{2.70}$$

The scattering matrix is unitary, satisfying $\mathcal{S}^\dagger \mathcal{S} = \mathbf{1}$. The transfer matrix $\mathcal{M}$ is *pseudo-unitary*, satisfying $\mathcal{M}^\dagger Z \mathcal{M} = Z$, with $Z = \mathsf{diag}(1, -1)$ is the Pauli σ^z matrix. This guarantees $|i|^2 - |o'|^2 =$

[37] J. T. Chalker and P. D. Coddington, *J. Phys. C: Solid State Phys.* **21**, 3665 (1988).

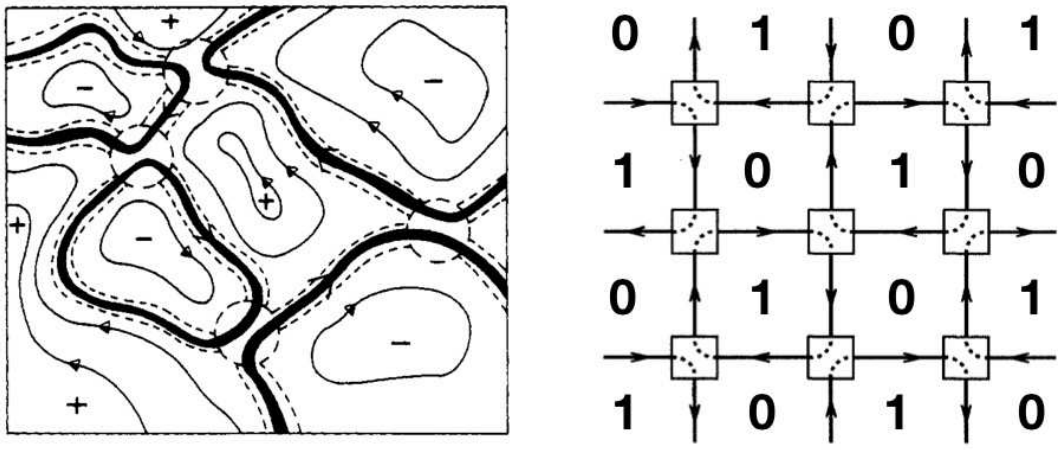

Figure 2.12: The Chalker-Coddington network model of quantum percolation. Left: Contour plots of a random potential $V(x,y)$. Local maxima and minima are denoted by $+$ and $-$ symbols. From J. T. Chalker and P. D. Coddington, *J. Phys. C: Solid State Phys.* **21**, 3665 (1988). Right: Idealized network of saddle points. Dashed curves show $\gamma \to \infty$ limit of the $\mathcal{S}$-matrix scattering (see text). From D.-H. Lee, Z. Wang, and S. Kivelson, *Phys. Rev. Lett.* **70**, 4130 (1993).

$|o|^2 - |i'|^2$ which is a restatement of current conservation $|o|^2 + |o'|^2 = |i|^2 + |i'|^2$. With $r = \sin(\theta)\, e^{i\psi}$ and $t = \cos(\theta)\, e^{i\omega}$, we have

$$\mathcal{M} = \begin{pmatrix} 1 & 0 \\ 0 & -e^{i(\psi+\delta)} \end{pmatrix} \begin{pmatrix} \sec\theta & \tan\theta \\ \tan\theta & \sec\theta \end{pmatrix} \begin{pmatrix} 1 & 0 \\ 0 & -e^{-i\psi} \end{pmatrix} e^{i\omega} \tag{2.71}$$

In the network model, flux amplitudes accrue random phases due to the varying lengths of the trajectories between saddles (see Eqn. 2.13), and the phases $e^{i\psi}$, $e^{i\omega}$, and $e^{i\delta}$ can be absorbed. Thus, we may take the transfer matrix at saddle point $\boldsymbol{r}$ to be

$$\mathcal{M}_{\boldsymbol{r}} = \begin{pmatrix} \sec\theta_{\boldsymbol{r}} & \tan\theta_{\boldsymbol{r}} \\ \tan\theta_{\boldsymbol{r}} & \sec\theta_{\boldsymbol{r}} \end{pmatrix} \equiv \begin{pmatrix} \cosh\gamma_{\boldsymbol{r}} & \sinh\gamma_{\boldsymbol{r}} \\ \sinh\gamma_{\boldsymbol{r}} & \cosh\gamma_{\boldsymbol{r}} \end{pmatrix} \tag{2.72}$$

with the identification $\cosh\gamma_{\boldsymbol{r}} \equiv \sec\theta_{\boldsymbol{r}}$ for $\theta_{\boldsymbol{r}} \in [0, \frac{\pi}{2}]$. While the parameter $\gamma_{\boldsymbol{r}}$ can vary from saddle to saddle, the simplest model takes $\theta_{\boldsymbol{r}} = \theta(E)$, hence $\gamma_{\boldsymbol{r}} = \gamma(E)$, to be the same energy-dependent value at all saddles. At $E = 0$, the reflection and transmission amplitudes are identical, hence $\theta(0) = \frac{\pi}{4}$ and $\gamma(0) = \ln\bigl(1+\sqrt{2}\bigr)$.

Linear chain of saddle points

The simplest case to consider involving many saddles is that of the linear chain, depicted in Fig. 2.14. This setting is essentially that from the Mil'nikov-Sokolov argument in §2.1.6. We

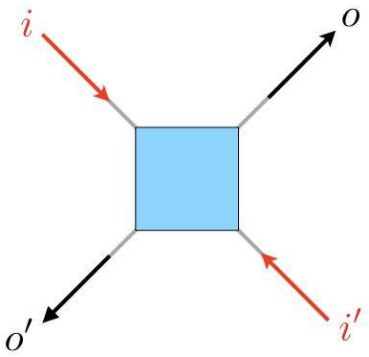

$$\begin{pmatrix} o' \\ o \end{pmatrix} = \mathcal{S} \begin{pmatrix} i \\ i' \end{pmatrix}$$

$$\begin{pmatrix} o \\ i' \end{pmatrix} = \mathcal{M} \begin{pmatrix} i \\ o' \end{pmatrix}$$

Figure 2.13: Relation between scattering ($\mathcal{S}$) and transfer ($\mathcal{M}$) matrices.

have, from the figure, $\Psi_{n+1} = U_n \, \mathcal{M}_n \, \Psi_n$, with

$$\overbrace{\begin{pmatrix} i_{n+1} \\ o'_{n+1} \end{pmatrix}}^{\Psi_{n+1}} = \overbrace{\begin{pmatrix} e^{i\alpha_n} & 0 \\ 0 & e^{-i\beta_n} \end{pmatrix}}^{U_n} \overbrace{\begin{pmatrix} \cosh\gamma_n & \sinh\gamma_n \\ \sinh\gamma_n & \cosh\gamma_n \end{pmatrix}}^{\mathcal{M}_n} \overbrace{\begin{pmatrix} i_n \\ o'_n \end{pmatrix}}^{\Psi_n} \quad . \tag{2.73}$$

where α_n and β_n are the phases accrued for the right- and left-moving flux amplitudes between saddles n and $n+1$. Thus, after N such saddles, we have $\Psi_{N+1} = \mathcal{Q}_N \, \Psi_1$, where the cumulative transfer matrix $\mathcal{Q}_N$ is given by

$$\mathcal{Q}_N \ = U_N \, \mathcal{M}_N \, \cdots \, U_2 \, \mathcal{M}_2 \, U_1 \, \mathcal{M}_1 \quad . \tag{2.74}$$

Suppose we wish to calculate the disorder average $\langle \, \Psi^\dagger_{N+1} \, A \, \Psi_{N+1} \, \rangle$, where $A = a_0 + \boldsymbol{a} \cdot \boldsymbol{\sigma}$ is an arbitrary 2×2 Hermitian matrix. Clearly $\langle \, \Psi^\dagger_{N+1} \, A \, \Psi_{N+1} \, \rangle = \Psi^\dagger_1 \, \langle \mathcal{Q}^\dagger_N \, A \, \mathcal{Q}_N \rangle \, \Psi_1$, so let us compute

$$\langle \mathcal{Q}^\dagger_N \, A \, \mathcal{Q}_N \rangle = \langle \, \mathcal{M}^\dagger_1 \, U^\dagger_1 \cdots \mathcal{M}^\dagger_N \, U^\dagger_N \, A \, U_N \, \mathcal{M}_N \cdots U_1 \, \mathcal{M}_1 \, \rangle \tag{2.75}$$

We start in the middle, first averaging over the random variables α_N and β_N, which are presumed to be independent and uniformly distributed over the circle. We have

$$\left\langle \begin{pmatrix} e^{-i\alpha_N} & 0 \\ 0 & e^{i\beta_N} \end{pmatrix} \begin{pmatrix} a_0 + a_3 & a_1 - i a_2 \\ a_1 + i a_2 & a_0 - a_3 \end{pmatrix} \begin{pmatrix} e^{i\alpha_N} & 0 \\ 0 & e^{-i\beta_N} \end{pmatrix} \right\rangle = \begin{pmatrix} a_0 + a_3 & 0 \\ 0 & a_0 - a_3 \end{pmatrix} \tag{2.76}$$

and

$$\begin{pmatrix} \cosh\gamma_N & \sinh\gamma_N \\ \sinh\gamma_N & \cosh\gamma_N \end{pmatrix} \begin{pmatrix} a_0 + a_3 & 0 \\ 0 & a_0 - a_3 \end{pmatrix} \begin{pmatrix} \cosh\gamma_N & \sinh\gamma_N \\ \sinh\gamma_N & \cosh\gamma_N \end{pmatrix} \tag{2.77}$$

$$= \begin{pmatrix} \cosh(2\gamma_N) \, a_0 + a_3 & \sinh(2\gamma_N) \, a_0 \\ \sinh(2\gamma_N) \, a_0 & \cosh(2\gamma_N) \, a_0 - a_3 \end{pmatrix} \quad .$$

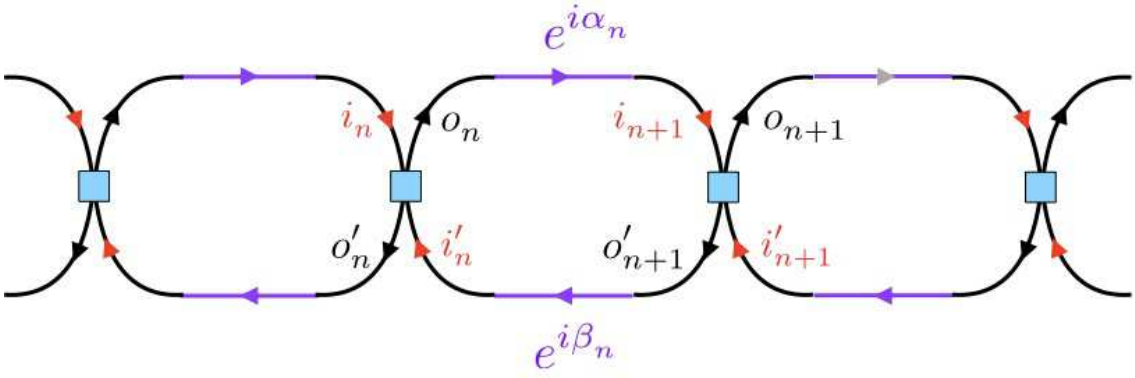

Figure 2.14: A chain of quantum saddle points.

Thus, we have the iterative rule

$$\begin{pmatrix} a'_0 \\ a'_1 \\ a'_2 \\ a'_3 \end{pmatrix} = \begin{pmatrix} \cosh(2\gamma_N)\, a_0 \\ \sinh(2\gamma_N)\, a_0 \\ 0 \\ a_3 \end{pmatrix} \tag{2.78}$$

and therefore

$$\left\langle\, \mathcal{Q}_N^\dagger \left(a_0\, 1 + \boldsymbol{a}\cdot\boldsymbol{\sigma}\right) \mathcal{Q}_N \,\right\rangle = \prod_{n=1}^{N} \cosh(2\gamma_N)\, a_0 \cdot \left(1 + \tanh(2\gamma_1)\, \sigma^1\right) + a_3\, \sigma^3 \quad . \tag{2.79}$$

Note that $\langle \mathcal{Q}_N^\dagger\, Z\, \mathcal{Q}_N \rangle = Z$, which is again the condition of current conservation. It is convenient to eliminate the σ^1 term by computing instead $\langle\, \Psi_{N+1}^\dagger\, A\, \Psi_{N+1}\,\rangle = \Phi_0^\dagger\, \langle U_0^\dagger\, \mathcal{Q}_N^\dagger\, A\, \mathcal{Q}_N\, U_0 \rangle\, \Phi_0$, where $\Phi_0^\dagger = \begin{pmatrix} o_0^* & i_0'^* \end{pmatrix}$, in which case

$$\left\langle\, U_0^\dagger\, \mathcal{Q}_N^\dagger \left(a_0\, 1 + \boldsymbol{a}\cdot\boldsymbol{\sigma}\right) \mathcal{Q}_N\, U_0 \,\right\rangle = \Lambda_N\, a_0\, 1 + a_3\, \sigma^3 \quad . \tag{2.80}$$

where $\Lambda_N \equiv \prod_{n=1}^{N} \cosh(2\gamma_n)$. With $\widetilde{\mathcal{Q}}_N \equiv \mathcal{Q}_N\, U_0$, we then have $\Psi_{N+1} = \widetilde{\mathcal{Q}}_N\, \Phi_0$, *i.e.*

$$\begin{pmatrix} i_{N+1} \\ o'_{N+1} \end{pmatrix} = \overbrace{\begin{pmatrix} 1/\mathsf{t}_N^* & -\mathsf{r}_N^*/\mathsf{t}_N^* \\ -\mathsf{r}_N\, e^{i\delta_N}/\mathsf{t}_N^* & e^{i\delta_N}/\mathsf{t}_N^* \end{pmatrix}}^{\widetilde{\mathcal{Q}}_N} \begin{pmatrix} o_0 \\ i'_0 \end{pmatrix} \quad . \tag{2.81}$$

From this we obtain

$$\begin{aligned} \left\langle |i_{N+1}|^2 \right\rangle &= \frac{\Lambda_N + 1}{2}\, |o_0|^2 + \frac{\Lambda_N - 1}{2}\, |i'_0|^2 \\ \left\langle |o'_{N+1}|^2 \right\rangle &= \frac{\Lambda_N - 1}{2}\, |o_0|^2 + \frac{\Lambda_N + 1}{2}\, |i'_0|^2 \quad , \end{aligned} \tag{2.82}$$

with $\frac{1}{2}(\Lambda_N + 1) = \langle 1/|\mathsf{t}_N|^2\rangle$. Note that terms proportional to $o_0^* i_0'$ do not enter on the RHS above because their coefficients $\langle \mathsf{r}/|\mathsf{t}|^2\rangle$ vanish because of the phase averaging. We identify the effective transmission and reflection coefficients by setting $o_{N+1} = 0$ and evaluating

$$\mathsf{T}_N \equiv \frac{\langle |i_{N+1}|^2\rangle}{|o_0|^2} = \frac{2}{\Lambda_N + 1} = \frac{1}{\langle 1/|\mathsf{t}_N|^2\rangle} \quad , \tag{2.83}$$

with $\mathsf{R}_N = 1 - \mathsf{T}_N$. If the $\{\gamma_n\}$ are randomly distributed, one must compute the corresponding average $\langle \Lambda_N\rangle = \langle \cosh(2\gamma)\rangle^N$ over the distribution $P(\gamma)$. The net result is that the transmission coefficient decays exponentially, as $\mathsf{T}_N \propto \exp(-N/\xi)$ with $\xi(\gamma) = 1/\ln\cosh(2\gamma)$. This is equivalent to one-dimensional Anderson localization. Note also that as defined $\mathsf{T}_N \neq \langle |\mathsf{t}_N|^2\rangle$.

Square lattice network model

Consider now the square lattice network model defined in Fig. 2.15. Each vertex is again described by a 2×2 $\mathcal{S}$-matrix as above, and the phases along the links act as 1×1 $\mathcal{S}$-matrices in the following manner:

$$\begin{aligned} o_{j+1\,,\,k} &= \exp(-i\,\alpha_{j\,,\,k})\, i'_{j\,,\,k} \\ i'_{j\,,\,k+1} &= \exp(i\,\beta_{j\,,\,k})\, o'_{j\,,\,k} \\ i_{j+2\,,\,k} &= \exp(i\,\alpha_{j+1\,,\,k})\, o'_{j+1\,,\,k} \\ o_{j+1\,,\,k+1} &= \exp(-i\beta_{j+1\,,\,k})\, i_{j+1\,,\,k} \quad , \end{aligned} \tag{2.84}$$

where $j + k$ is even, corresponding to the blue vertices in the figure. At each vertex, we have

$$\begin{pmatrix} o' \\ o \end{pmatrix} = \begin{pmatrix} -\sin\theta & \cos\theta \\ \cos\theta & \sin\theta \end{pmatrix} \begin{pmatrix} i \\ i' \end{pmatrix} \qquad \Longleftrightarrow \qquad \begin{pmatrix} o \\ i' \end{pmatrix} = \begin{pmatrix} \sec\theta & \tan\theta \\ \tan\theta & \sec\theta \end{pmatrix} \begin{pmatrix} i \\ o' \end{pmatrix} \quad . \tag{2.85}$$

In the γ parameterization, recall that $\cosh\gamma = \sec\theta$, *i.e.* $\gamma = \ln(\sec\theta + \tan\theta)$. When $\theta = 0$ ($\gamma = 0$) we have $o = i$ and $o' = i'$, *i.e.* perfect transmission. In Fig. 2.15, this corresponds to clockwise motion around $\nu > \frac{1}{2}$ regions, *i.e.* $E > 0$. When $\theta = \frac{\pi}{2}$ ($\gamma = \infty$), we have $o' = -i$ and $o = i'$, *i.e.* perfect reflection, corresponding to counterclockwise motion around $\nu < \frac{1}{2}$ regions.

In the numerical work by Lee, Wang, and Kivelson (LWK)[38], the scattering parameter γ was given by $\gamma_{\boldsymbol{r}} = \gamma_{\rm c}\exp(\mu - V_{\boldsymbol{r}})$, where $\gamma_{\rm c} = \ln(1+\sqrt{2})$ is the critical value (corresponding to $\theta = \frac{\pi}{4}$), μ is a dimensionless chemical potential, and $V_{\boldsymbol{r}}$ is a dimensionless local random potential distributed uniformly on the interval $[-W, W]$. The system is arranged in a $L \times M$ rectangular lattice, with the M direction periodic. By applying the $\mathcal{S}$-matrices at each vertex and along the links, one can numerically derive an $M \times M$ transfer matrix $\mathcal{T}(L, M, \mu)$ which acts on the leftmost column of M flux amplitudes to generate the rightmost column of M flux amplitudes[39],

[38] D.-H. Lee, Z. Wang, and S. Kivelson, *Phys. Rev. Lett.* **70**, 4130 (1993).

[39] We assume L and M are even.

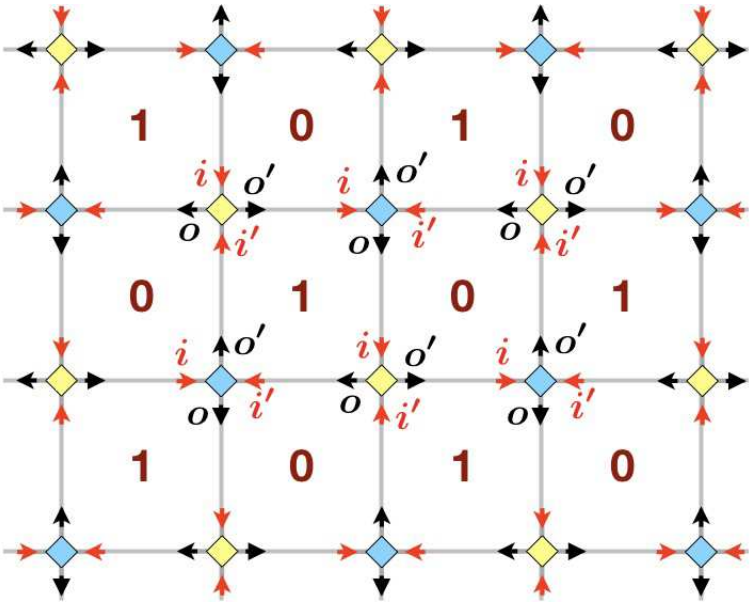

Figure 2.15: The square lattice Chalker-Coddington network model. Plaquettes marked with 0 correspond to $\nu < \frac{1}{2}$ regions, while plaquettes marked with 1 correspond to $\nu > \frac{1}{2}$ regions.

viz.

$$\begin{pmatrix} o'_1(L) \\ \vdots \\ o'_{M/2}(L) \\ i'_1(L) \\ \vdots \\ i'_{M/2}(L) \end{pmatrix} = \mathcal{T} \begin{pmatrix} i_1(1) \\ \vdots \\ i_{M/2}(L) \\ o_1(L) \\ \vdots \\ o_{M/2}(L) \end{pmatrix} \quad . \tag{2.86}$$

Note that if $P(\lambda) = \det(\lambda - \mathcal{T})$ is the characteristic polynomial of $\mathcal{T}$, then $\mathcal{T}^\dagger Z \mathcal{T} = Z$, where $Z = \mathrm{diag}(1, \ldots, 1, -1, \ldots, -1) = 1_{M/2} \oplus (-1)_{M/2}$ is a diagonal $M \times M$ matrix, then

$$P(\lambda) = \lambda^M \det(\lambda^{-1} - \mathcal{T}^*) / \det(\mathcal{T}^*) \quad , \tag{2.87}$$

which establishes that the roots of $P(\lambda)$ come in pairs $(\lambda_j, 1/\lambda_j^*)$, where without loss of generality we may assume $|\lambda_j| \geq 1$ for $j \in \{1, \ldots, \frac{1}{2}M\}$. If the eigenvalues $\lambda_j(L, M, \mu)$ of $\mathcal{T}(L, M, \mu)$ are ordered such that $1 \leq |\lambda_1| \leq \cdots \leq |\lambda_{M/2}|$, then we define the $j^{\rm th}$ *localization length* $\xi_j(M, \mu)$ as the (inverse of the) positive real quantity

$$\xi_j^{-1}(M, \mu) \equiv \lim_{L \to \infty} \frac{1}{L} \ln \big| \lambda_j(L, M, \mu) \big| \quad . \tag{2.88}$$

As defined, we have $M/2$ localization lengths, ordered according to $\xi_1(M, \mu) \geq \cdots \geq \xi_{M/2}(M, \mu)$. We are interested in the largest localization length, *i.e.* for $j = 1$. In the limit $W \to \infty$, the parameter γ is finite with vanishing probability, and the classical percolation limit is recovered.

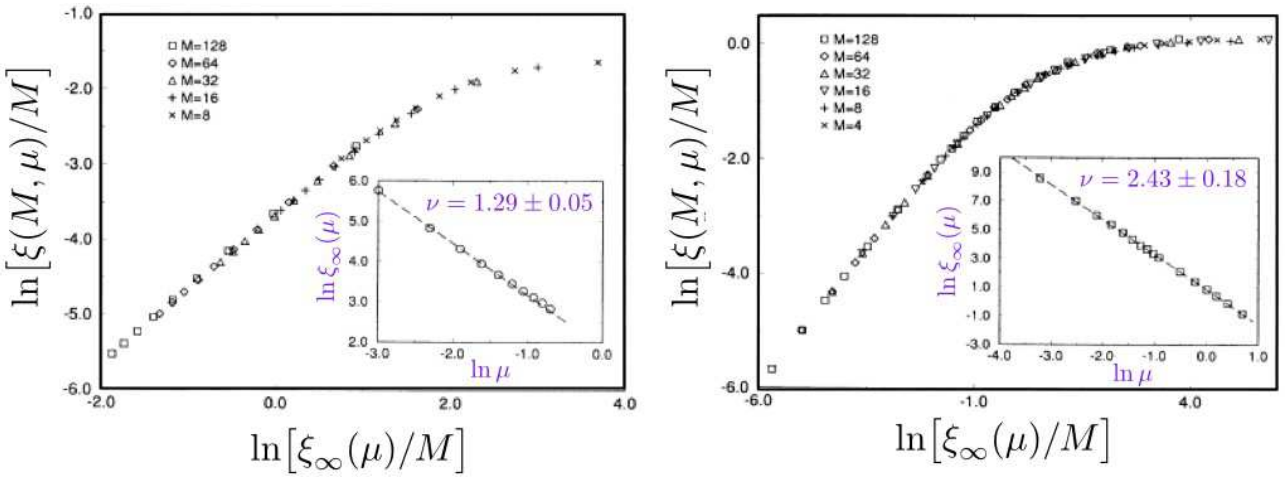

Figure 2.16: Scaling determination of exponent ν for classical and quantum 2D percolation. From D.-H. Lee, Z. Wang, and S. Kivelson, *Phys. Rev. Lett.* **70**, 4130 (1993).

For quantum percolation, LWK set $W = 1$. LWK examined systems with $L = 2 \times 10^5$ and with M ranging from 8 to 128. Finite size scaling theory says that when $L \gg M$, one can write

$$\xi(M,\mu) = M F(\xi_\infty(\mu)/M) \quad , \tag{2.89}$$

where F is a scaling function and where $\xi_\infty(\mu)$ is the thermodynamic localization length. To obtain $\xi_\infty(\mu)$, one plots $\ln\left[\xi(M,\mu)/M\right]$ *versus* $\ln(1/M)$ for different values of μ and then shifts the curve for each μ by an amount such that the curves all overlap. The amount of the shift is then identified with $\ln \xi_\infty(\mu)$. This method yields both the thermodynamic localization length $\xi_\infty(\mu)$ as well as the scaling function F.

2.2.4 Tight-binding and other models of the disordered Landau Level

Other numerical investigations of the IQH transition have utilized a Hamiltonian approach, where when projected on the $n^{\rm th}$ Landau level the Hamiltonian matrix elements are

$$H_{nk_1,nk_2} = (n + \tfrac{1}{2})\hbar\omega_{\rm c}\,\delta_{k_1,k_2} + \langle\, n,k_1 \,|\, V \,|\, n,k_2 \,\rangle \quad , \tag{2.90}$$

where $V(\boldsymbol{r})$ is the random potential and $k_{1,2}$ are the y-wavevectors in the Landau strip basis. Because the Landau strip spacing is $\Delta x = 2\pi\ell^2/L_y$, in the limit $L_y \to \infty$, the random potential couples many different strip wavefunctions, leading to a long-ranged one-dimensional hopping problem in the k_y basis, where, please recall, $\exp(ik_yL_y) = 1$. Another lattice model is the disordered Hofstadter model, whose real space matrix elements are given by

$$H_{\boldsymbol{r},\boldsymbol{r}'} = -t\, e^{iA_{\boldsymbol{r}\boldsymbol{r}'}} + W_{\boldsymbol{r}}\,\delta_{\boldsymbol{r},\boldsymbol{r}'} \quad , \tag{2.91}$$

with $A_{r'r} = -A_{rr'}$, and where the directed (counterclockwise) sum of the gauge potential $A_{rr'}$ along nearest neighbor links $\langle rr' \rangle$ around a plaquette p gives the dimensionless flux ϕ_p. Typically one then computes the lattice Green's function for this model,

$$G_{r,r'}(E) = \langle\, r \,|\, \frac{1}{E + i\epsilon - H} \,|\, r' \,\rangle \tag{2.92}$$

as a function of energy E and fixed dimensionless ratio W/t, where W is the width of the distribution of the $\{W_r\}$. On a strip of length L and width M, the longest localization length is given by the expression

$$\xi^{-1}(M, E) = -\lim_{L\to\infty} \lim_{\epsilon\to 0} \frac{1}{2L} \left\langle \ln \sum_{i,j=1}^{M} \left| G_{1i,Lj}(E) \right|^2 \right\rangle \quad , \tag{2.93}$$

where $i, j \in \{1, \ldots, M\}$ label the transverse coordinate[40]. The approach of using Green's functions to numerically compute localization lengths was pioneered by MacKinnon and Kramer in the early 1980s[41]. The scaling theory of the IQH transition has been reviewed by B. Huckestein[42]. A computational advantage of this method over exact diagonalization is that the Green's function can be computed recursively. Very recently, Puschmann *et al.*[43] obtained $\nu = 2.58(3)$ in studies of the disordered square lattice Hofstadter model, consistent with Slevin and Ohtsuki's network model result $\nu = 2.593 \pm 0.006$[44]. Note that this rules out the Mil'nikov-Sokolov result $\nu_{\rm QU} = \frac{7}{3}$, which is in fact closer to the experimentally determined value of ν.

Zhu, Wu, Bhatt, and Wan[45], building on earlier work of Huo and Bhatt[46], investigated a disordered square lattice Hofstadter model, equivalent to Eqn. 2.91, with $\phi = \frac{2\pi}{3}$ per structural unit cell. In the absence of disorder, this yields three Landau subbands $|\psi_n(\boldsymbol{\theta})\rangle$, with Chern numbers $+1$, 0, and -1, for $n = 1, 2$, and 3, respectively. They then considered the truncated model where the disorder potential W_r is projected onto the $n = 1$ subband of the disorder-free model, *i.e.*

$$H(\boldsymbol{\theta}, \boldsymbol{\theta}') = \sum_{\boldsymbol{\theta},\boldsymbol{\theta}'} |\, \psi_1(\boldsymbol{\theta}) \,\rangle\langle\, \psi_1(\boldsymbol{\theta}) \,|\, W_{\boldsymbol{r}} \,|\, \psi_1(\boldsymbol{\theta}') \,\rangle\langle\, \psi_1(\boldsymbol{\theta}') \,| \quad , \tag{2.94}$$

where $\theta_{1,2} = (2\pi j_{1,2} + \zeta)_{1,2})/N_{1,2}$, where $j_{1,2} \in \{1, \ldots, N_{1,2}\}$ and where $\alpha_{1,2} \in [0, 2\pi]$. Note we could also denote $H(\boldsymbol{\theta}, \boldsymbol{\theta}') = H_{\boldsymbol{j},\boldsymbol{j}'}(\boldsymbol{\zeta})$. There are then $N_1 N_2$ eigenstates $|\, \varphi_l(\boldsymbol{\zeta}) \,\rangle$ for each pair of boundary phases $(\zeta)_1, \zeta)_2)$, and the Chern numbers are given by

$$C_l = \frac{i}{2\pi} \int_{\mathsf{T}^2} d^2\zeta\, \epsilon_{\alpha\beta} \left\langle \frac{\partial \varphi_l}{\partial \zeta^\alpha} \,\middle|\, \frac{\partial \varphi_l}{\partial \zeta^\beta} \right\rangle \tag{2.95}$$

[40] In systems of higher dimension $d > 2$ and of size $M \times \cdots \times M \times L$, one writes $i \to \boldsymbol{r}_\perp$ and $j \to \boldsymbol{r}'_\perp$, and the sum is over all $M^{2(d-1)}$ pairs $(\boldsymbol{r}_\perp, \boldsymbol{r}'_\perp)$.

[41] See A. MacKinnon and B. Kramer, *Phys. Rev. Lett.* **47**, 1546 (1981). For application to the IQHE, see B. Huckestein and B. Kramer, *Phys. Rev. Lett.* **64**, 1437 (1990).

[42] B. Huckestein, *Rev. Mod. Phys.* **67**, 357 (1995).

[43] M. Puschmann, P. Cain, M. Schreiber, and T. Vojta, *Phys. Rev. B* **99**, 121301(R) (2019).

[44] K. Slevin and T. Ohtsuki, *Phys. Rev. B* **80**, 041304 (2009)

[45] Q. Zhu, P. Wu, R. N. Bhatt, and X. Wan, *Phys. Rev. B* **99**, 024205 (2019).

[46] Y. Huo and R. N. Bhatt, *Phys. Rev. Lett.* **68**, 1375 (1992).

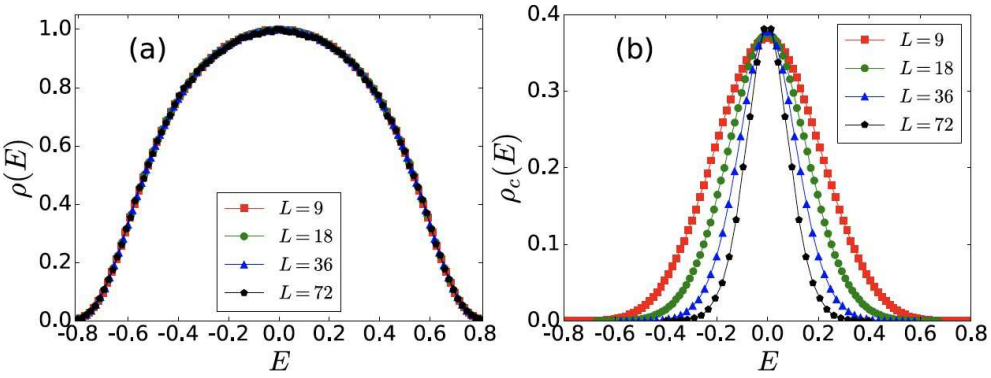

Figure 2.17: Disorder-averaged DOS and DOCS (density of conducting states). From Q. Zhu, P. Wu, R. N. Bhatt, and X. Wan, *Phys. Rev. B* **99**, 024205 (2019).

where the integral is over the torus $\boldsymbol{\zeta} \in [0, 2\pi] \times [0, 2\pi]$. Zhu *et al.* computed both the disorder-averaged density of states $\rho(E)$ as well as the disorder-averaged density of conducting states $\rho_{\rm c}(E)$, defined as

$$\begin{aligned} \rho(E) &= \left\langle \frac{1}{N_1 N_2} \sum_{l=1}^{N_1 N_2} \delta(E - E_l) \right\rangle \\ \rho(E) &= \left\langle \frac{1}{N_1 N_2} \sum_{l=1}^{N_1 N_2} (1 - \delta_{C_l,0})\, \delta(E - E_l) \right\rangle \quad , \end{aligned} \tag{2.96}$$

where the second sum includes contributions only from states of nonzero Chern number. Their results are shown in Fig. 2.17. As the linear system size $N_1 = N_2 \equiv L$ is increased, the width of $\rho(E)$ remains unchanged, but that of $\rho_{\rm c}(E)$ narrows, indicating that in the thermodynamic limit a sub-extensive number of states carry nonzero Chern number. A scaling *Ansatz*, with $N_{\rm c} = a\, N_\phi^{-1/(2\nu)}$, where $N_\phi = N_1 N_2\, \phi = \frac{2\pi}{3} L^2$, was analyzed, and good agreement was found with $\nu = 2.49 \pm 0.01$[47]. The form of the scaling *Ansatz* is inspired by the fact that one expects that for system of linear size $L \propto \sqrt{N_\phi}$, states with $\xi(E) > L$ are conducting. The number of these states scales as $N_{\rm c} \sim L^2 \rho(E_{\rm c})\, |E - E_{\rm c}|$ with $\xi(E) = L$, hence $|E| \propto L^{-1/\nu}$, and $E_{\rm c} = 0$ for symmetrically distributed disorder. Thus, $N_{\rm c} \propto L^{2-1/\nu} \propto N_\phi^{1-1/(2\nu)}$.

2.2.5 Real Space Renormalization

Symmetry dictates that a square lattice Chalker-Coddington (CC) network model composed of identical scatterers with $\gamma_r = \gamma$ should exhibit a quantum critical point at $\gamma = \gamma_{\rm c} = \ln(1+\sqrt{2})$, *i.e.* at $T = R = \frac{1}{2}$, where T and R are the transmission and reflection coefficients for each individual

[47] The authors also investigated corrections to scaling, with $N_{\rm c}/N_\phi = a(1 + bN_\phi^{-\gamma/2})N_\phi^{-1/(2\nu)}$, which gave better agreement, with $\nu = 2.480 \pm 0.005$.

vertex. Consider now the case where $T = \mathrm{sech}\,\gamma$ at each site is chosen from a distribution $P(T)$, and consider the problem of transmission through an $L \times L$ lattice of saddle point vertices. One may (at least numerically) compute the distribution $P_L(T)$ of transmission (defined, say, from left to right) across this system, averaging over all the link phases. In the limit $L \to \infty$, one expects two stable distributions, given by $P_\infty(T) = \delta(T)$ and $P_\infty(T) = \delta(1-T) = \delta(R)$, corresponding to bulk localized phases with $T = 0$ and $T = 1$, respectively. The word "stable" in this context alludes to a notional renormalization group (RG) flow. As we have discussed above in §2.2.2, applications of RG techniques to the replica field theory of the IQHE have been intractable due to difficulties associated with the topological term and the $n \to 0$ replica limit. Here we describe a real space RG approach to the IQH transition based on the network model, following D. P. Arovas, M. Janssen, and B. Shapiro, *Phys. Rev. B* **56**, 1751 (1997), henceforth denoted as ABS97[48]. Real space RG (RSRG) schemes have the virtue of being easily implemented and physically appealing, but suffer from being completely uncontrolled and not providing any systematic way to calculate critical properties with increasing accuracy (such as going to more loops in diagrammatic field theory calculations)[49]. As applied to the CC network model, the RSRG approach obtains the distribution $P_{bL}(T)$ for a larger system of linear dimension bL in terms of $P_L(T)$. This functional relation may be represented in terms of a set of parameters $\{X_i(L)\}$ which characterize the distribution $P_L(T)$, such as the coefficients in a Chebyshev or Legendre polynomial expansion of $P_L(T)$ in the variable $x = 2T - 1$. Thus, one has

$$X_i(bL) = F_i\big(\{X_j(L)\}; b\big) \quad . \tag{2.97}$$

The fixed point distribution is then characterized by $\{X_i^*\}$, where $X_i^* = F_i\big(\{X_j^*\}; b\big)$, and the eigenvalues $\{\lambda_a\}$ of the matrix $R_{ij} = \big(\partial F_i/\partial X_j\big)_{\boldsymbol{X}^*}$ determine the relevance of the corresponding eigenvectors, which are the *scaling variables*. The positive eigenvalues define a set of critical exponents, $y_a = \ln \lambda_a / \ln b$ and the localization length exponent $\nu = \ln b / \ln \lambda_{\rm min}$ corresponds to the smallest eigenvalue $\lambda_{\rm min}$. The β-functions are defined to be

$$\beta_i\big(\{X_j\}\big) = \frac{\partial X_i}{\partial \ln L} = \left.\frac{\partial F_i}{\partial b}\right|_{b=1} \quad . \tag{2.98}$$

In order to implement this program exactly, one would need to compute the distribution $P_L(T)$ for finite networks of arbitrary size. This is an intractable problem for even modest $L \sim 10$, hence one must resort to some approximation scheme, which is the source of all troubles with the RSRG approach. Here we will briefly describe two such approximation schemes: (i) Migdal-Kadanoff (MK) decimation, and (ii) hierarchical lattice constructions. Both allow for a recursive implementation of the RSRG program, using only simple numerical computation.

In Fig. 2.13, we saw how the scattering matrix $\mathcal{S}$, which gives the linear relation between incoming flux amplitudes (i, i') and outgoing flux amplitudes (o, o'), can be recast as a transfer

[48] See also A. G. Galstyan and M. E. Raikh, *Phys. Rev. B* **56**, 1422 (1997).

[49] Truth be told, with the trivial exception of $d = 1$, RSRG schemes generally yield poor results for critical exponents.

matrix $\mathcal{M}$, relating data (i, o') on the left of the vertex to data (o, i') on the right. Similarly, one can define a transfer matrix $\mathcal{N}$ which relates data (i, o) above the vertex to data (o', i') below the vertex. Thus,

$$\begin{pmatrix} o' \\ o \end{pmatrix} = \mathcal{S} \begin{pmatrix} i \\ i' \end{pmatrix} \quad \Leftrightarrow \quad \begin{pmatrix} o \\ i' \end{pmatrix} = \mathcal{M} \begin{pmatrix} i \\ o' \end{pmatrix} \quad \Leftrightarrow \quad \begin{pmatrix} o' \\ i' \end{pmatrix} = \mathcal{N} \begin{pmatrix} i \\ o \end{pmatrix} \quad . \tag{2.99}$$

In particular,

$$\mathcal{S} = \begin{pmatrix} -\sin\theta & \cos\theta \\ \cos\theta & \sin\theta \end{pmatrix} \quad \Leftrightarrow \quad \mathcal{M} = \begin{pmatrix} \sec\theta & \tan\theta \\ \tan\theta & \sec\theta \end{pmatrix} \quad \Leftrightarrow \quad \mathcal{N} = \begin{pmatrix} -\csc\theta & \operatorname{ctn}\theta \\ -\operatorname{ctn}\theta & \csc\theta \end{pmatrix} \quad . \tag{2.100}$$

Note $\mathcal{S}^\dagger \mathcal{S} = 1$ and $\mathcal{M}^\dagger Z \mathcal{M} = \mathcal{N}^\dagger Z \mathcal{N} = Z$. Now consider the combination of two scatterers in series, as depicted in the left panel of Fig. 2.18. The combined transfer matrix is given by

$$\mathcal{M}' = \mathcal{M}_2 \, U \, \mathcal{M}_1 = \begin{pmatrix} \sec\theta_2 & \tan\theta_2 \\ \tan\theta_2 & \sec\theta_2 \end{pmatrix} \begin{pmatrix} e^{i\alpha} & 0 \\ 0 & e^{-i\beta} \end{pmatrix} \begin{pmatrix} \sec\theta_1 & \tan\theta_1 \\ \tan\theta_1 & \sec\theta_1 \end{pmatrix} \quad . \tag{2.101}$$

Computing $\sec^2\theta' = |\mathcal{M}'_{1,1}|^2 = 1/T'$, we obtain the transmission coefficient

$$\frac{1}{T'} = \frac{1 + 2\sqrt{R_1 R_2}\,\cos(\alpha+\beta) + R_1 R_2}{T_1 T_2} \quad . \tag{2.102}$$

Averaging $\ln T$ over the angle $\phi \equiv \alpha + \beta$, we obtain $\langle \ln T' \rangle = 2 \langle \ln T \rangle$, and for b scatterers in series,

$$\langle \ln T' \rangle = b \, \langle \ln T \rangle \quad . \tag{2.103}$$

Thus $\ln T$ is driven to increasingly negative values under iteration, which is the essence of one-dimensional localization.

Equivalently, though, we may construct the transfer matrix from "top to bottom", in which case

$$\mathcal{N}' = \mathcal{N}_2 \, U \, \mathcal{N}_1 = \begin{pmatrix} -\csc\theta_2 & \operatorname{ctn}\theta_2 \\ -\operatorname{ctn}\theta_2 & \csc\theta_2 \end{pmatrix} \begin{pmatrix} e^{i\alpha} & 0 \\ 0 & e^{-i\beta} \end{pmatrix} \begin{pmatrix} -\csc\theta_1 & \operatorname{ctn}\theta_1 \\ -\operatorname{ctn}\theta_1 & \csc\theta_1 \end{pmatrix} \quad . \tag{2.104}$$

But now $\csc^2\theta' = |\mathcal{N}'_{1,1}|^2 = 1/R'$, and we have

$$\frac{1}{R'} = \frac{1 + 2\sqrt{T_1 T_2}\,\cos(\alpha+\beta) + T_1 T_2}{R_1 R_2} \quad . \tag{2.105}$$

This yields

$$\langle \ln R' \rangle = b \, \langle \ln R \rangle \tag{2.106}$$

for b scatterers in parallel. In this case it is the reflection amplitude which is driven to zero! In the network model, both series as well as parallel propagation are present, and in a sense it is the competition between these two one-dimensional localization mechanisms which gives rise to a quantum critical point describing the IQH transition. Tractably separating the series and parallel processes, however, can only be implemented in approximation schemes such as MK or hierarchical lattice constructions.

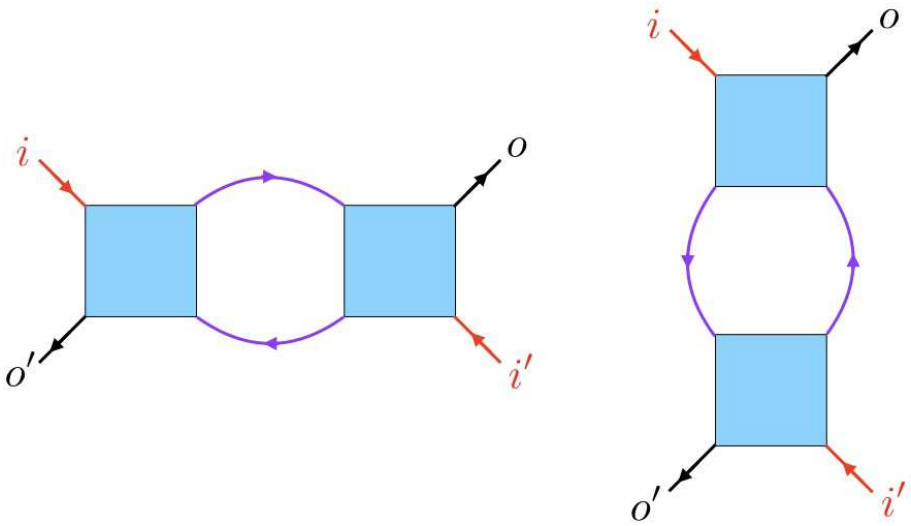

Figure 2.18: Series (left) and parallel (right) two-channel quantum scatterers.

Migdal-Kadanoff method

The Migdal-Kadanoff decimation scheme involves "bond-shifting" and is represented graphically in Fig. 2.19. To understand how this leads to critical behavior, consider the behavior of the *typical* transmission coefficient $\mathsf{T} \equiv \exp\langle \ln T \rangle$. From the above series and parallel computations, we have $\mathsf{T}_b = \mathsf{T}^b$ for series and $\mathsf{R}_b = \mathsf{R}^b$ for parallel transmission. The renormalized vertex for $b = 2$ after bond-shifting is shown in the upper right panel of Fig. 2.19, and corresponds to parallel transmission between two series pairs of the original vertices. For arbitrary b, then,

$$\mathsf{T}' = 1 - (1 - \mathsf{T}^b)^b \equiv f(\mathsf{T}; b) \quad . \tag{2.107}$$

For $b = 2$, we have $f(\mathsf{T}; b = 2) = 2\mathsf{T}^2 - \mathsf{T}^4$. This map has two stable fixed points at $\mathsf{T}^* = 0$ and 1, and an unstable fixed point at $\mathsf{T}^* = \frac{1}{2}(\sqrt{5} - 1) \simeq 0.618$. Linearizing about the unstable fixed point, we obtain the eigenvalue

$$\lambda = \left. \frac{\partial f(\mathsf{T}; b = 2)}{\partial \mathsf{T}} \right|_{\mathsf{T}^*} = 6 - 2\sqrt{5} \quad , \tag{2.108}$$

corresponding to a localization length exponent $\nu = \ln b / \ln \lambda \simeq 1.635$. Note that $\mathsf{T}^* \neq \frac{1}{2}$ because the order of the bond shifting matters[50]. Choosing instead parallel followed by series propagation, rather than series followed by parallel, the roles of T and R are reversed[51].

[50] Thus, the composite vertex in Fig. 2.19 is not invariant under 90° rotations.

[51] The RG equation in Eqn. 2.108 and its $\mathsf{T} \leftrightarrow \mathsf{R}$ counterpart coincide with the two RSRG equations obtained in the MK approach to classical bond percolation. There, the bond occupation probability p plays the role of our T, and the MK bond-shifting which in our model leads to a series or parallel composition of quantum resistors corresponds to multiplication of bond occupation probabilities. See S. R. Kirkpatrick, *Phys. Rev. B* **15**, 1533 (1977).

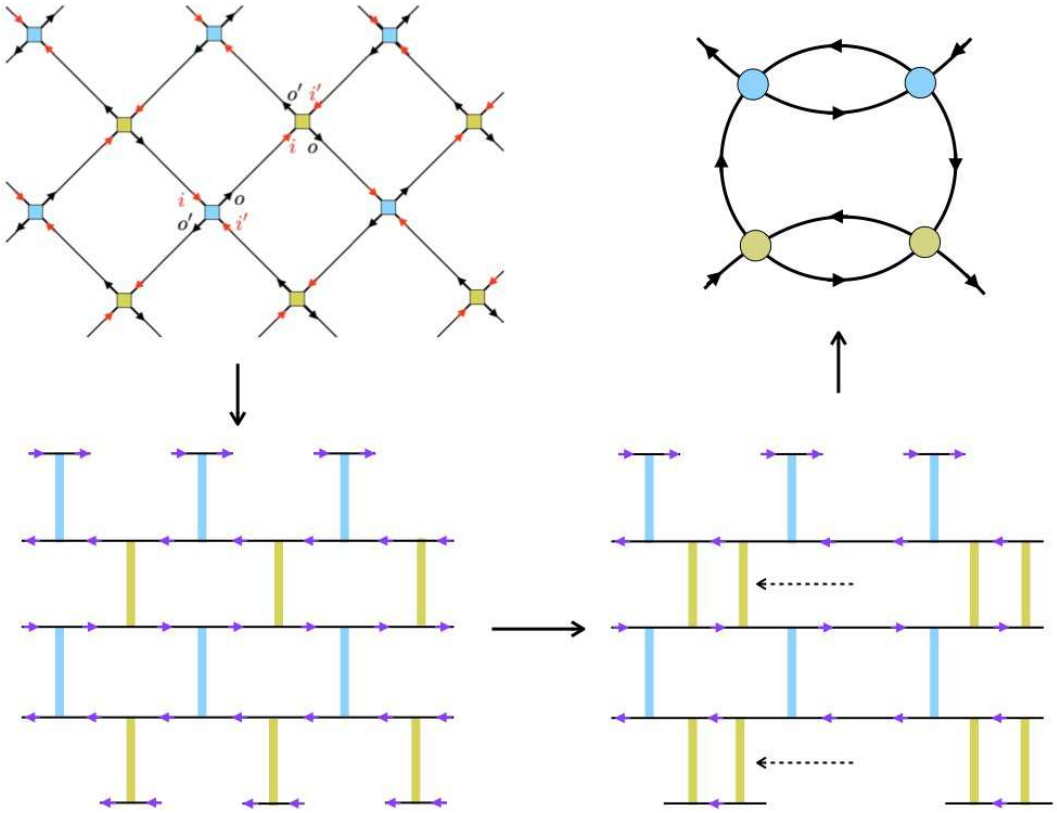

Figure 2.19: Migdal-Kadanoff decimation of the Chalker-Coddington network model. In the first stage of the decimation, the CC network is represented as a "brick lattice". A $b = 2$ bond-shifting process effectively replaces each single vertex with a group of two vertices in series. In the second stage of the decimation, the brick lattice is represented in the orthogonal (y) direction. Bond-shifting then replaces each composite vertex from stage one with a new composite vertex arising first from serial and then parallel propagation. The resulting composite vertex for $b = 2$ is shown in the upper right portion of the figure.

If we set $b = 1 + \zeta$ with $\zeta \downarrow 0$, we obtain the "infinitesimal" MK transformation,

$$\mathsf{T}' = \mathsf{T} + \zeta\big[\mathsf{T}\ln\mathsf{T} - (1-\mathsf{T})\ln(1-\mathsf{T})\big] + \mathcal{O}(\zeta^2) \quad , \tag{2.109}$$

The infinitesimal MK transformation again has fixed points at $\mathsf{T} = 0$ and $\mathsf{T} = 1$, and its unstable fixed point lies at the symmetric value $\mathsf{T} = \frac{1}{2}$, with eigenvalue $\lambda = 2(1 - \ln 2)\zeta$, corresponding to $\nu = \big[2(1 - \ln 2)\big]^{-1} \simeq 1.629$. The β-function is

$$\beta(\mathsf{T}) = \frac{\partial f(\mathsf{T}; 1+\zeta)}{\partial\zeta}\bigg|_{\zeta=0} = \mathsf{T}\ln\mathsf{T} - (1-\mathsf{T})\ln(1-\mathsf{T}) \quad . \tag{2.110}$$

Note that $\beta(\mathsf{T}^*) = 0$ vanishes at the fixed points, where there is no RSRG flow.

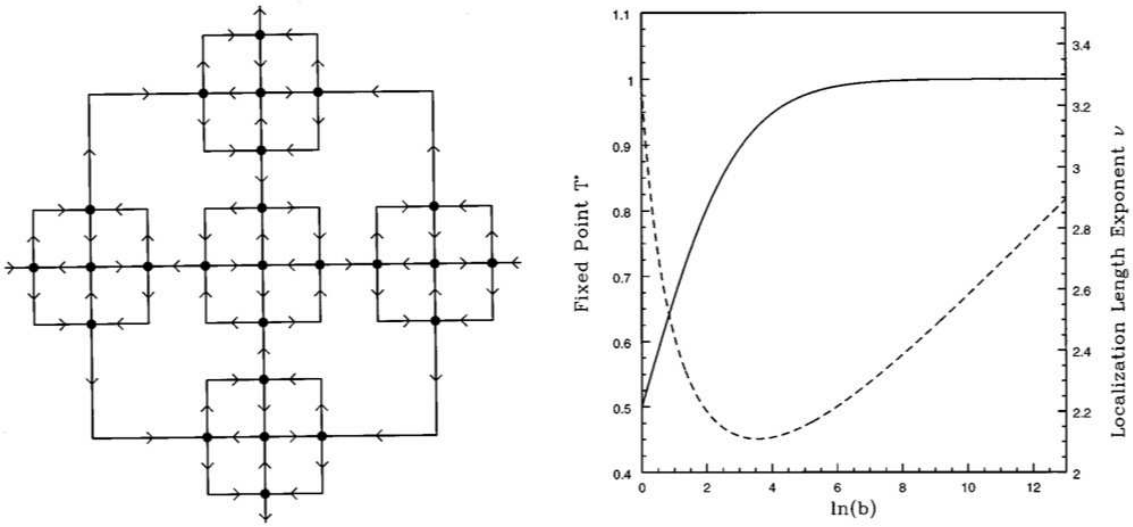

Figure 2.20: Left: A hierarchical lattice at the second stage of construction. Right: Results for a hierarchical lattice construction generalizing that in the left panel, but when the central site is replaced by a unit S-matrix. From D. P. Arovas, M. Janssen, and B. Shapiro, *Phys. Rev. B* **56**, 1751 (1997).

Hierarchical lattice constructions

A related approach to the problem involves the artifice of hierarchical lattices, which are systems of noninteger Hausdorff dimension. Consider, for example, the system depicted in the left panel of Fig. 2.20. The elementary motif is a group of $V = 5$ vertices chosen from a 3×3 ($M = 3$) group of sites, where the scatterers at the four corners are removed. This configuration is arranged into a repeating structure at ever larger length scales. Repeating this process n times results in a hierarchical structure with V^n vertices contained in a square of side length M^n. The Hausdorff dimension is t$D_{\rm H} = \ln V / \ln M$, hence $D_{\rm H}(V = 5, M = 3) \simeq 1.465$; generalizations to $V(M) = \frac{1}{2}(M^2 + 1)$ can be constructed, for which the limiting Hausdorff dimension is $\lim_{M\to\infty} D_{\rm H}(M) = 2$. To recover the previous MK scheme, replace the central scatterer with one for which $T = 1$, resulting in the four site composite vertex of Fig. 2.19. Results from the hierarchical lattice construction are shown in the right panel of Fig. 2.20.

If one replaces the central scatterer in the left panel of Fig. 2.20 with one for which $S = 1$ (perfect transmission), one recovers the four-site scattering unit of Fig. 2.19. One can use this as the fundamental unit of a hierarchical construction, and the results differ from those of the previous section only in that the linear dimension is taken to be $M = 2b - 1$ rather than $M = b$. The Hausdorff dimension of the hierarchical lattice is then $D_{\rm H} = \ln(b^2)/\ln M = 2\ln b/\ln(2b-1)$ ($= \ln 4/\ln 3 = 1.2619$ for the case $b = 2$), whereas the bond-shifted MK lattice is fully two-dimensional. The correlation length exponent ν is accordingly different, and given by $\nu = \ln(2b-1)/\ln\lambda$. For $b = 2$ one has $\nu = \ln 3/\ln(6 - 2\sqrt{5}) = 2.592$, which is shockingly (and surely fortuitously) close to the current best numerical value $\nu = 2.58$. Generalizations to larger b are

straightforward and results are shown in the right panel of Fig. 2.20 (see ABS97 for details).

2.2.6 Spin-orbit coupling

The microscopic Hamiltonian for a single electron in a potential $V(\boldsymbol{r})$ and magnetic field $\boldsymbol{B}$ is

$$H = \frac{\boldsymbol{\pi}^2}{2m_{\rm e}} + V(\boldsymbol{r}) + \frac{e\hbar}{2m_{\rm e}c}\,\boldsymbol{\sigma}\cdot\boldsymbol{B} + \frac{\hbar}{4m_{\rm e}^2c^2}\,\boldsymbol{\sigma}\cdot\boldsymbol{\nabla}V\times\boldsymbol{\pi} + \frac{\hbar^2}{8m_{\rm e}^2c^2}\boldsymbol{\nabla}^2V + \frac{(\boldsymbol{\pi}^2)^2}{8m_{\rm e}^3c^2} + \ldots\ , \tag{2.111}$$

where $\boldsymbol{\pi} = \boldsymbol{p} + \frac{e}{c}\boldsymbol{A}$. Where did this come from? From the Dirac equation,

$$i\hbar\frac{\partial\Psi}{\partial t} = \begin{pmatrix} m_{\rm e}c^2 + V & c\,\boldsymbol{\sigma}\cdot\boldsymbol{\pi} \\ c\,\boldsymbol{\sigma}\cdot\boldsymbol{\pi} & -m_{\rm e}c^2 + V \end{pmatrix}\Psi = E\Psi\ . \tag{2.112}$$

The wavefunction Ψ is a four-component Dirac spinor. Since $m_{\rm e}c^2$ is the largest term for our applications, the upper two components of Ψ are essentially the positive energy components. However, the Dirac Hamiltonian mixes the upper two and lower two components of Ψ. One can 'unmix' them by making a canonical transformation, $H \longrightarrow H' \equiv e^{iS}\,H\,e^{-iS}$, where S is Hermitian, to render H' block diagonal. With $E = m_{\rm e}c^2 + \varepsilon$, the effective Hamiltonian is given by (2.111). This is known as the Foldy-Wouthuysen transformation, the details of which may be found in many standard books on relativistic quantum mechanics and quantum field theory (*e.g.* Bjorken and Drell, Itzykson and Zuber, *etc.*). Note that the Dirac equation leads to $g = 2$. If we go beyond "tree level" and allow for radiative corrections within QED, we obtain a perturbative expansion, $g = 2 + \frac{\alpha}{\pi} + \mathcal{O}(\alpha^2)$, where $\alpha = e^2/\hbar c \approx 1/137$ is the fine structure constant.[52] There are two terms in (2.111) which involve the electron's spin[53]:

$$\begin{aligned} \text{Zeeman interaction}\ :\ H_{\rm Z} &= \frac{ge\hbar}{4m_{\rm e}c}\,\boldsymbol{\sigma}\cdot\boldsymbol{B} \\ \text{Spin-orbit interaction}\ :\ H_{\rm SO} &= \frac{\hbar^2}{4m_{\rm e}^2c^2}\,\boldsymbol{\sigma}\cdot\boldsymbol{\nabla}V\times\left(\boldsymbol{k} + \tfrac{e}{\hbar c}\boldsymbol{A}\right)\quad . \end{aligned} \tag{2.113}$$

We define $\lambda_0 \equiv \hbar^2/4m_{\rm e}c^2 = 3.7\times10^{-6}\,\text{Å}^2$ to be the vacuum SO coupling parameter.

In crystalline solids, spin-orbit effects can be profound for large Z ions[54]. For crystalline GaAs, as well as for Si and Ge, near the Γ point in the Brillouin zone, the antibonding conduction band s-orbitals are split by the band gap Δ from the bonding valence band p-orbitals[55].

[52] Note that with $\mu_{\rm n} = e\hbar/2m_{\rm p}c$ for the nuclear magneton, $g_{\rm p} = 2.793$ and $g_{\rm n} = -1.913$. These results immediately suggest that there is composite structure to the nucleons, *i.e.* quarks.

[53] The numerical value for $\mu_{\rm B}$ is $\mu_{\rm B} = e\hbar/2mc = 5.788\times10^{-9}\,\text{eV/G}$, hence $\mu_{\rm B}/k_{\rm B} = 6.717\times10^{-5}\,\text{K/G}$.

[54] For a thorough discussion of spin-orbit effects in solids, see R. Winkler, *Spin-Orbit Coupling Effects in Two-Dimensional Electron and Hole Systems* (Springer, 2003).

[55] In Si and Ge, the conduction band minimum at Γ is not the lowest energy point in the conduction band.

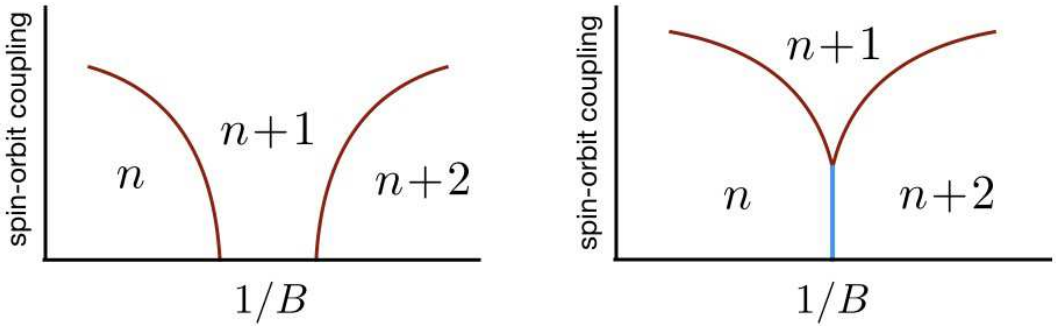

Figure 2.21: Possible phase diagrams for the disordered Landau level with spin-orbit coupling. Left: Two distinct transitions, each with $\kappa = 1/\nu z \simeq 0.42$. Right: One merged transition at sufficiently weak SO disorder scattering, with $\kappa \simeq 0.21$.

Including electron spin, these amount to eight states. When spin-orbit effects are included, the six valence band orbitals rearrange themselves into light and heavy hole bands which are degenerate at Γ, and a lower energy *split-off hole* band, where the splitting $\Delta_{\rm so}$ is due to spin-orbit effects. In a crystalline energy band and in the presence of a disorder potential $V_{\rm imp}(\boldsymbol{r})$ arising from impurities, the effective Hamiltonian is

$$H_{\rm eff} = \frac{\hbar^2}{2m^*}\big(\boldsymbol{k} + \tfrac{e}{\hbar c}\boldsymbol{A}\big)^2 + V_{\rm imp}(\boldsymbol{r}) + \frac{g^* e\hbar}{4m_{\rm e}c}\,\boldsymbol{\sigma}\cdot\boldsymbol{B} + \lambda\,\boldsymbol{\sigma}\cdot\boldsymbol{\nabla}V_{\rm imp}\times\big(\boldsymbol{k} + \tfrac{e}{\hbar c}\boldsymbol{A}\big) \quad , \tag{2.114}$$

which is of the same form as the expression in vacuum, but where the coupling λ is now material-dependent. For the conduction band of GaAs, for example, $\lambda = 5.3\,\text{Å}^2$, which is 10^6 times larger than the vacuum value λ_0[56].

We now ask: what happens when we include spin degrees of freedom in the IQH transition? First note that the Zeeman energy splits $\uparrow$ and $\downarrow$ spin states by $\Delta_{\rm Z} = \zeta\hbar\omega_{\rm c}$, where $\zeta \equiv g^* m^*/2m_{\rm e}$. In other words, with $V_{\rm imp}(\boldsymbol{r}) = 0$ the energy eigenvalues are $E_{n\sigma} = (n + \frac{1}{2} + \frac{1}{2}\sigma\zeta)\hbar\omega_{\rm c}$. Due to the effects of band structure and confinement in quantum wells, the g-factor can vary considerably from its tree level QED value of $g = 2$. Values as high as $g^* = 60$ have been observed in InAs/AlSb quantum wells, and g can also be tuned by pressure – in some cases to $g^* = 0$.

Consider the case of a single cyclotron Landau level with $a^\dagger a = n$ and $\sigma = \pm 1$. In the absence of SO coupling, and with weak disorder $V(\boldsymbol{r}) \equiv V_{\rm imp}(\boldsymbol{r})$ coupling only to density and not to spin, there are two independent transitions. What happens when the $\uparrow$ and $\downarrow$ spin components are mixed through the SO coupling term in H? Khmelnitskii[57] argued that the extended states of overlapping Landau spin subbands should split, and network model simulations by Lee and Chalker[58] support this conclusion, and that the localization length $\xi(E)$ thus diverges at two distinct energies. Polyakov and Shklovskii[59] further argued that if the two extended state

[56] See B. I. Halperin, *2005 Boulder Summer School for Condensed Matter and Materials Physics* lecture notes.
[57] D. E. Khmelnitskii, *Helv. Phys. Acta* **65**, 164 (1992).
[58] D. K. K. Lee and J. T. Chalker, *Phys. Rev. Lett.* **72**, 1510 (1994).
[59] D. G. Polyakov and B. I. Shklovskii, *Phys. Rev. Lett.* **70**, 3796 (1993).

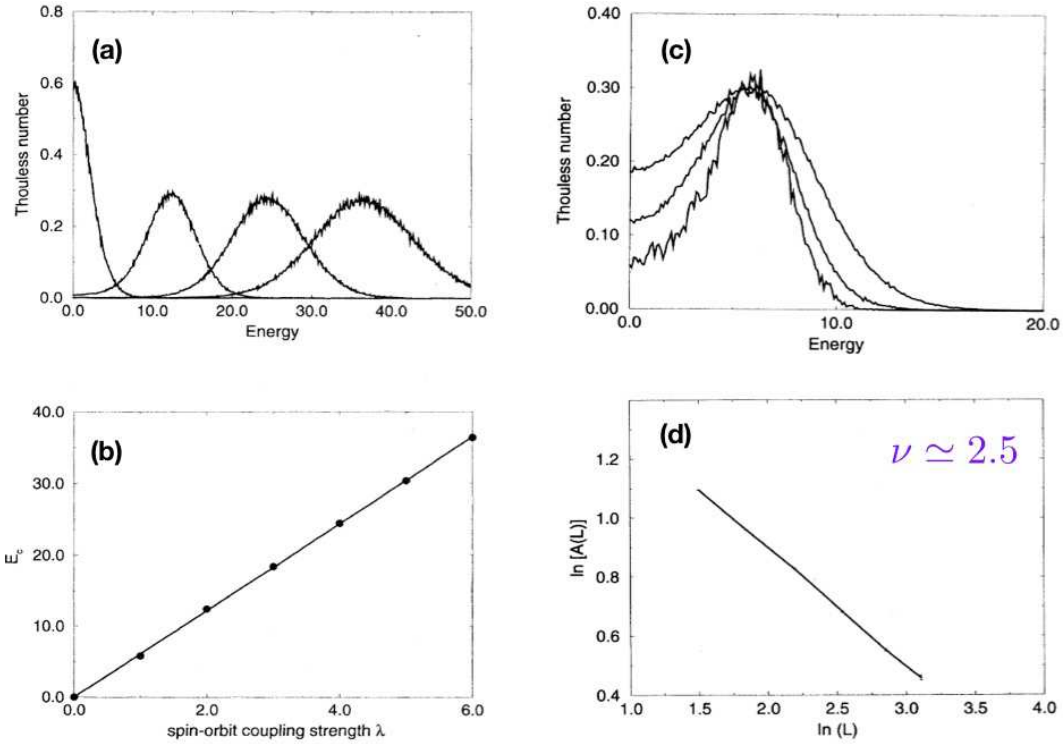

Figure 2.22: (a) Thouless number data for smooth SO scattering ($\zeta = 2$) for $N_\phi = 40$, 60, 160, and 500. (b) Log-log plot of the integrated area under the Thouless number curves $T_L(E)$ *versus* system size. The resulting slope yields $\nu \approx 2.5$. (c) Thouless number for smooth SO scattering ($\zeta = 2$) as a function of energy for coupling strengths $\lambda = 0$, 2, 4, and 6. (d) Tracking of the Thouless number peak, with $E_c(\lambda) \propto \lambda W$. From C. B. Hanna *et al.*, *Phys. Rev. B* **52**, 5221 (1995).

energies lie at $E = \pm E_c$, then the localization length should take the form

$$\xi(E) \propto \left(\frac{\Gamma^2}{|E^2 - E_c^2|} \right)^\nu \quad , \tag{2.115}$$

where Γ is the disorder broadening of the LLs, which is assumed to satisfy $\Gamma \gg E_c$. This would suggest a crossover behavior where the actual correlation length exponent ν is observed only very close to $E = \pm E_c$, and at sufficiently low temperatures. Otherwise, $\xi \sim |\Gamma/E|^{2\nu}$ and an apparent doubling of the exponent is predicted. Such an apparent doubling of the exponent for spin-degenerate peaks was reported in microwave measurements[60], where the width of the transition is observed to scale as $\Delta B \propto \omega^\gamma$, where $\gamma = 1/\nu z$ if the quantum critical point view of the transition pertains. For isolated peaks, $\gamma = 0.41 \pm 0.04$ was found, while for spin-degenerate peaks, $\gamma = 0.20 \pm 0.05$. The reader is advised to note our descriptive collocation, "*apparent* doubling" (italics for stress).

[60] L. W. Engel *et al.*, *Phys. Rev. Lett.* **71**, 2638 (1993).

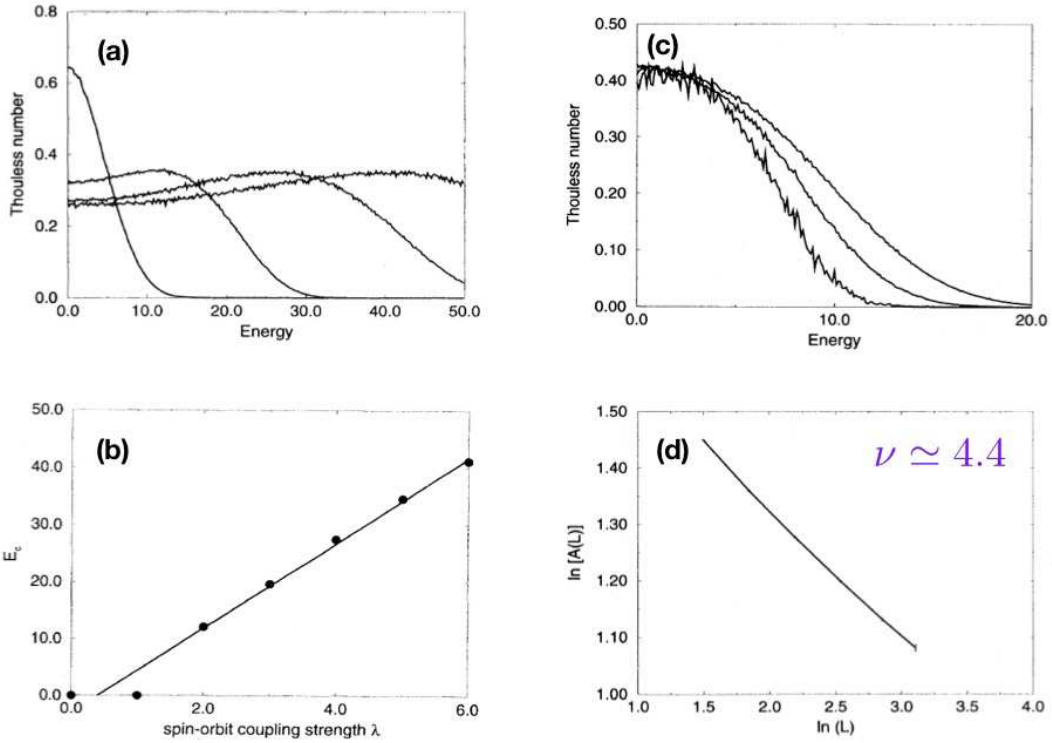

Figure 2.23: (a) Thouless number data for white noise SO scattering ($\zeta = 0$) for $N_\phi = 40, 60, 160,$ and 500. (b) Log-log plot of the integrated area under the Thouless number curves $T_L(E)$ *versus* system size. The resulting slope yields $\nu \approx 4.4$. (c) Thouless number for smooth SO scattering ($\zeta = 2$) as a function of energy for coupling strengths $\lambda = 0$, 2, 4, and 6. (d) Tracking of the Thouless number peak, with $E_{\rm c}(\lambda) \propto \lambda W$. From C. B. Hanna *et al. op. cit.*.

Hanna *et al.*[61] (HAMG) studied the model

$$H = \Pi_0 \left[V(\boldsymbol{r}) + \lambda \, \boldsymbol{W}(\boldsymbol{r}) \cdot \boldsymbol{\sigma} \right] \Pi_0 \quad , \tag{2.116}$$

where Π_0 projects onto the $n = 0$ cyclotron Landau level, where $V(\boldsymbol{r})$ and $W_{x,y,z}(\boldsymbol{r})$ are Gaussian random fields of zero mean, satisfying

$$\begin{aligned} \big\langle V(\boldsymbol{r})\, V(\boldsymbol{r}') \big\rangle &= \frac{V^2}{2\pi\zeta^2} \, \exp\big(-|\boldsymbol{r} - \boldsymbol{r}'|^2/2\zeta^2 \big) \\ \big\langle W_\alpha(\boldsymbol{r})\, W_\beta(\boldsymbol{r}') \big\rangle &= \frac{W^2}{2\pi\zeta^2} \, \exp\big(-|\boldsymbol{r} - \boldsymbol{r}'|^2/2\zeta^2 \big) \, \delta_{\alpha\beta} \quad , \end{aligned} \tag{2.117}$$

where V and W are the respective strengths of the scalar and spin-dependent random potentials, and ζ is the correlation length of the disorder, assumed the same for both $V(\boldsymbol{r})$ and $\boldsymbol{W}(\boldsymbol{r})$. The limit $\zeta \to 0$ corresponds to Gaussian white noise, but is effectively smoothed on the scale of

[61] C. B. Hanna, D. P. Arovas, K. Mullen, and S. M. Girvin, *Phys. Rev. B* **52**, 5221 (1995).

the magnetic length ℓ due to the LLL projection Π_0. Note that there is no Zeeman term, corresponding to $g^* = 0$, hence the spins in the absence of the $\boldsymbol{W} \cdot \boldsymbol{\sigma}$ term are completely unresolved. In other words,

$$H_{j\alpha,j'\alpha'}(\theta_1,\theta_2) = \langle\, j \,|\, V(\boldsymbol{r}) \,|\, j' \,\rangle\, \delta_{\alpha\alpha'} + \lambda \,\langle\, j \,|\, \boldsymbol{W}(\boldsymbol{r}) \,|\, j' \,\rangle \cdot \boldsymbol{\sigma}_{\alpha\alpha'} \quad , \tag{2.118}$$

where (θ_1, θ_2) are the boundary condition Bloch phases. HAMG computed the *Thouless number*, which, for the $n^{\rm th}$ state in the spectrum, is defined to be

$$T_n = \overline{g(E_n)}\,\big|E_n(\pi,0) - E_n(0,0)\big| \quad , \tag{2.119}$$

where $\overline{g(E_n)}$ is the density of states at energy E_n, averaged over some width δE which contains many levels. The energy difference $\Delta E = E_n(\pi,0) - E_n(0,0)$ is the difference between values at antiperiodic and periodic boundary conditions in the θ_1 phase[62]. One finds $T_n = T(E_n)$ is a smooth function of the energy E_n after averaging over disorder. Assuming the scaling form

$$T_L(E) = f\big(\xi(E)/L\big) \equiv \tilde{f}(L^{1/\nu}|E|) \quad , \tag{2.120}$$

the area under the $T_L(E)$ curves behaves as

$$A(L) = \int\limits_{-\infty}^{\infty} dE\, T_L(E) = C\, L^{-1/\nu} \quad , \tag{2.121}$$

where $T_L(0)$ and C are independent of the system size L.

HAMG found that for smooth SO disorder scattering ($\zeta = 2$), there are indeed two fully resolved individual peaks of $T_L(E)$ located at $E = \pm E_{\rm c}$, with $E_{\rm c}$ independent of L for $L \gtrsim 40$ (see Fig. 2.22). The dependence of $E_{\rm c}$ on the SO coupling λ was found to be linear. Plotting $\ln A(L)$ *versus* $\ln L$, an exponent of $\nu \approx 2.5$ was extracted. Results white noise disorder ($\zeta = 0$) are shown in Fig. 2.23. The two peaks of $T_L(E)$ are poorly resolved, and an attempt to infer ν from the scaling *Ansatz* for $T_L(E)$ yields the approximately doubled value $\nu \simeq 4.4$. Much larger systems are apparently necessary in order to fully resolve the two peaks and to obtain the presumably correct value of $\nu \approx 2.5$.

2.3 Edge States

Recall the Hofstadter model from §1.6.2. Rather than applying doubly periodic boundary conditions in both x and y directions, consider the model on a cylinder with N_1 sites on each row parallel to the symmetry axis, and N_2 sites in the periodic direction. We will take $N_2 \to \infty$ but keep N_1 finite. A sketch is given in Fig. 2.24. The boundaries at the edges of the cylinder break

[62] One could equally well define the Thouless number with respect to boundary conditions in the θ_2 phase.

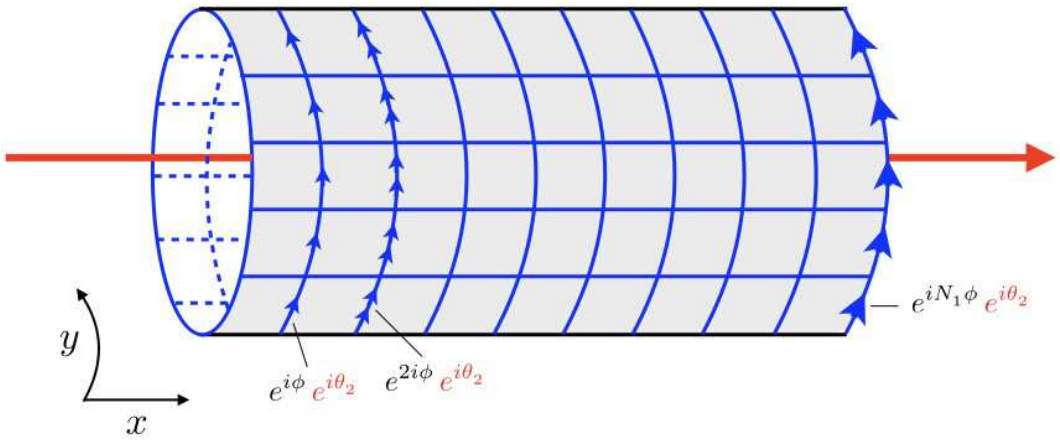

Figure 2.24: Hofstadter model on a cylinder, with flux ϕ per unit cell.

translational invariance in the x-direction, so the magnetic unit cell is now $N_x \times 1$ structural unit cells, and the Hamiltonian is

$$H(\theta_2, N_1, z) = -t \begin{pmatrix} 2\cos\theta_2 & 1 & 0 & \cdots & z^* \\ 1 & 2\cos(\theta_2+\phi) & 1 & & 0 \\ 0 & 1 & \ddots & & \vdots \\ \vdots & & & & 1 \\ z & 0 & \cdots & 1 & 2\cos(\theta_2 + N_1\phi) \end{pmatrix} , \tag{2.122}$$

which is an $N_1 \times N_1$ matrix. Here z controls the boundary condition in the x-direction, with $z = \exp(iN_1\theta_1/q)$ for periodic (toroidal) boundary conditions and $z = 0$ for open (cylindrical) boundary conditions.

For the infinite square lattice Hofstadter model with flux $\phi = 2\pi p/q$ per structural unit cell, TKNN showed that the Chern number C_r for the $r^{\rm th}$ subband is given by $C_r = t_r - t_{r-1}$, where $t_0 = 0$ and where t_r is determined by the solution of the Diophantine equation[63]

$$r = q\, s_r + p\, t_r \quad . \tag{2.123}$$

with $|t_r| \leq \frac{1}{2}q$. For $p = 3$ and $q = 7$, one has $r = 7s_r + 3\, t_r$ and the solutions to the TKNN Diophantine equation are given by

$$\begin{aligned} &(s_1, t_1) = (1, -2) \quad , \quad (s_2, t_2) = (-1, 3) \quad , \quad (s_3, t_3) = (0, 1) \quad , \quad (s_4, t_4) = (1, -1) \\ &(s_5, t_5) = (2, -3) \quad , \quad (s_6, t_6) = (0, 2) \quad , \quad (s_7, t_7) = (1, 0) \quad . \end{aligned} \tag{2.124}$$

The t_r values are $(t_0, \ldots, t_7) = (0, -2, +3, +1, -1, -3, +2, 0)$ and thus the Chern numbers are found to be $(C_1, \ldots, C_7) = (-2, +5, -2, -2, -2, +5, -2)$.

[63] Our convention corresponds to TKNN's strong potential limit.

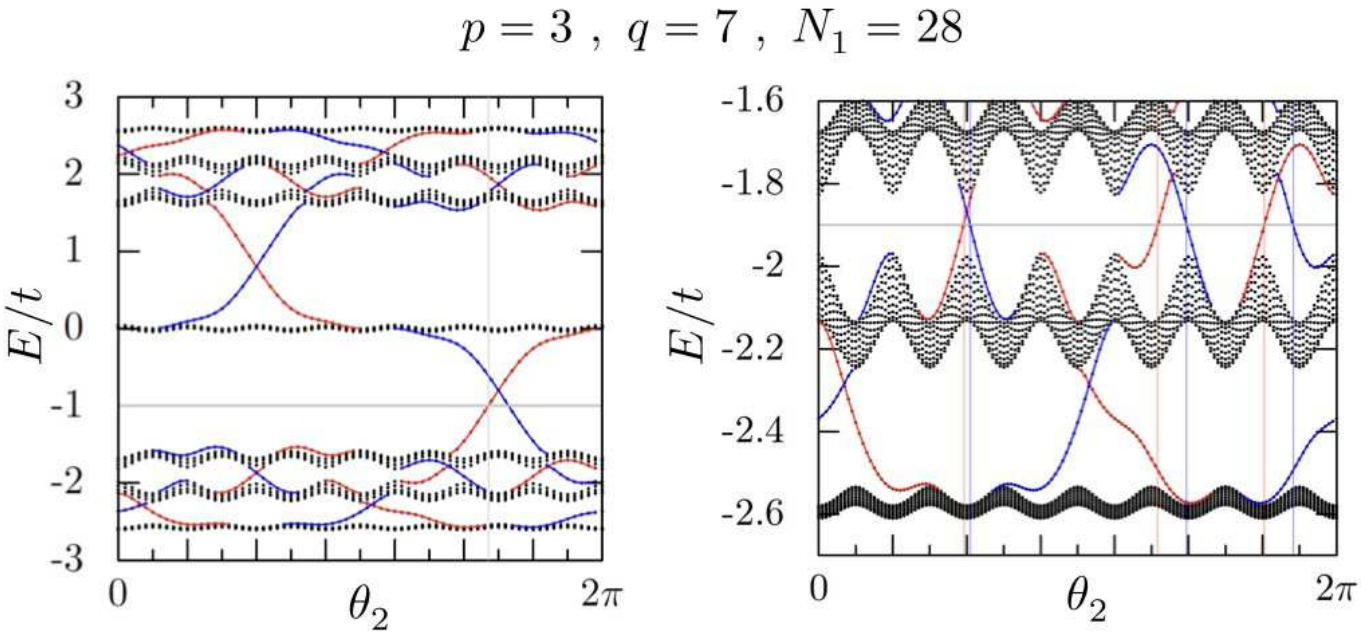

Figure 2.25: Left: bulk bands and edge states for the Hofstadter model with $p = 3$, $q = 7$, and $N_1 = 4q = 28$. Light vertical lines indicate θ_2 values corresponding to edge state crossings of the Fermi level (light horizontal line). Right: Detail of lowest three bulk bands and their associated edge states.

Consider now the results for the finite cylinder with $N_1 = 28$ shown in Fig. 2.25. Notice an essential difference relative to the bulk spectra: isolated energy levels traverse the gaps. These are *edge states* localized along either the left boundary of the cylinder (shown in red) or the right boundary (shown in blue). From the relation $\hbar v_2 = a\,\partial E/\partial\theta_2$, where a is the lattice constant, we see that the direction of each edge mode is determined by the sign of the slope of its dispersion curve whenever the Fermi level lies in a gap between bulk bands. Note that the modes associated with a given edge do not always propagate in the same direction as they do in the continuum (corresponding to the case $q \to \infty$), but can switch direction as the Fermi level is placed in consecutive bulk gaps.

Now look closely at Fig. 2.25 and note that there are two red edge levels propagating with $v_2 < 0$ when E_{F} lies in the gap between bands $r = 1$ and $r = 2$. This corresponds to the value $t_1 = -2$ obtained from the TKNN Diophantine equation above. When E_{F} lies in the gap between bulk bands $r = 2$ and $r = 3$, we see there are three red edge levels with $v_2 > 0$, corresponding to $t_2 = +3$, again in agreement with TKNN. Examining the next gap, we find $t_3 = +1$. In general, we observe the rule that *the Chern number C_r of the r^{th} band is the difference in the number of clockwise propagating states on the left edge when the Fermi level is changed from the $(r+1)^{\text{th}}$ to the r^{th} gap between bulk subbands*.

This correspondence between the bulk Chern number and the edge state structure is true in

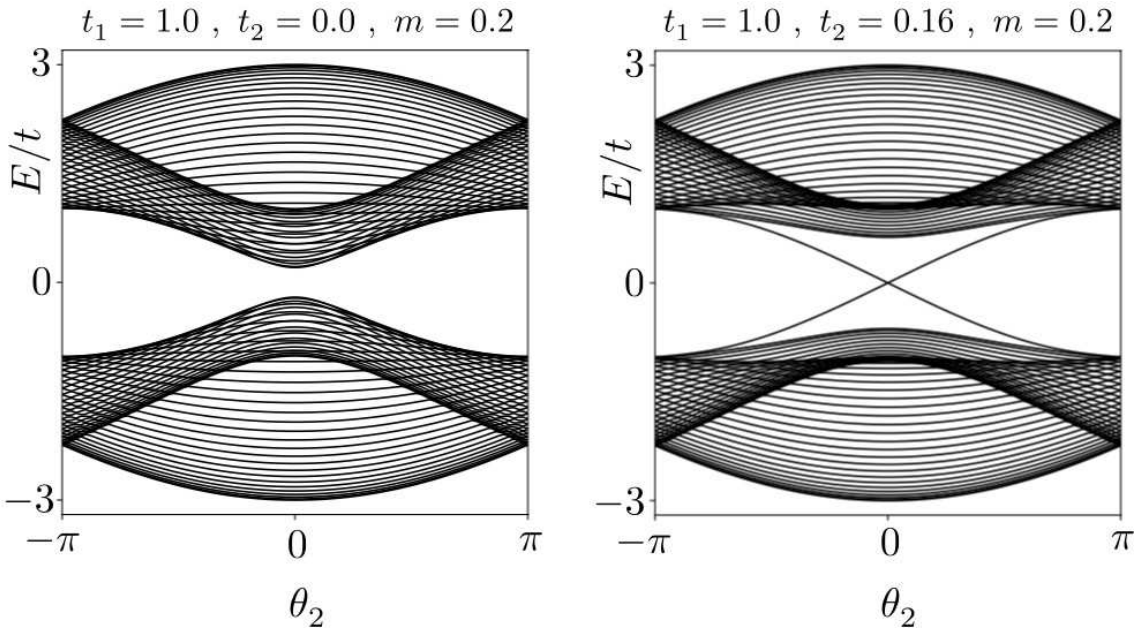

Figure 2.26: Bulk bands and edge states for the Haldane honeycomb lattice model with $t_1 = 1.0$ and $m = 0.2$. Left: $t_2 = 0$ (nontopological). Right: $t_2 = 0.16 > m/3\sqrt{3}$ (topological). Credit: https://topocondmat.org/w4_haldane/haldane_model.html.

general, and for another example consider the case of the Haldane honeycomb lattice model discussed in §1.7.3. When placed on a cylinder, the energy levels as a function of the Bloch phase θ_2 are depicted in Fig. 2.26, both in the nontopological $\big(|t_2| < |m|/3\sqrt{3}\big)$ and topological $\big(|t_2| > |m|/3\sqrt{3}\big)$ phases. Note how edge levels interpolating between the bulk bands are present in the topological phase, where the bulk band Chern numbers are $C_\pm = \mp 1$. Any lattice model with nonzero total Chern index when the Fermi level lies in a bulk gap is known as a *Chern insulator*.

2.3.1 Hatsugai's formulation

Yasuhiro Hatsugai in 1993 provided a particularly lucid description of the mathematics of edge states in lattice Chern insulators[64]. Consider a square lattice Chern insulator on a cylinder of dimensions $N_x \times N_y$, where y is the periodic direction, and where we take $N_y \to \infty$. Translational invariance in y guarantees that k_y is a good quantum number, and as usual we define $\theta_2 \equiv k_y a$, where a is the lattice constant. Let us fix our interest on the Hofstadter model with flux $\phi = 2\pi p/q$ per structural unit cell, and let $N_x = Jq$ where J is a positive integer. The

[64] Y. Hatsugai, *Phys. Rev. Lett.* **71**, 3697 (1993); Y. Hatsugai, *Phys. Rev. B* **48**, 11581 (1993).

wavefunction is described by the set of functions $\{\psi_n(\theta_2)\}$, where $n \in \{0, \ldots, N_x\}$.

$$\begin{aligned} \text{toroidal} \ : \ & \psi_{n+N_x}(\theta_2) = \psi_n(\theta_2) \ \forall \ n \\ \text{cylindrical} \ : \ & \psi_0(\theta_2) = \psi_{N_x}(\theta_2) = 0 \quad . \end{aligned} \tag{2.125}$$

In the toroidal case, choosing a $q \times 1$ magnetic unit cell, we have $\psi_{n+q}(\theta_2) = e^{i\theta_1}\psi_n(\theta_2)$ with $\theta_1 = 2\pi j/J$ and $j \in \{1, \ldots, J\}$.

The lattice Schrödinger equation for the Hofstadter model is

$$-t\,\psi_{n-1} - 2t\cos(n\phi + \theta_2)\,\psi_n - t\,\psi_{n+1} = E\,\psi_n \quad , \tag{2.126}$$

which may be restated as

$$\begin{pmatrix} \psi_{n+1} \\ \psi_n \end{pmatrix} = \overbrace{\begin{pmatrix} -\varepsilon - 2\,\cos(n\phi + \theta_2) & -1 \\ 1 & 0 \end{pmatrix}}^{R_n(\varepsilon, \theta_2, \phi)} \begin{pmatrix} \psi_n \\ \psi_{n-1} \end{pmatrix} \quad , \tag{2.127}$$

with $\varepsilon \equiv E/t$. We define the transfer matrix

$$M(\varepsilon) \equiv R_q(\varepsilon) R_{q-1}(\varepsilon) \cdots R_1(\varepsilon) \quad , \tag{2.128}$$

where we suppress notation of θ_2 and ϕ for clarity. The full transfer matrix across the cylinder is then $M^J(\varepsilon)$, and given our boundary condition $\psi_0(\theta_2) = 0$, we have

$$\begin{pmatrix} \psi_{Jq+1} \\ \psi_{Jq} \end{pmatrix} = M^J(\varepsilon) \begin{pmatrix} 1 \\ 0 \end{pmatrix} \quad . \tag{2.129}$$

This requires $\big[M^J(\varepsilon)\big]_{21} = 0$, which is a degree $N_x - 1 = Jq - 1$ polynomial equation in ε for each θ_2. Writing

$$N_x - 1 = (N_x - q) + (q - 1) = (J - 1)\,q + (q - 1) \quad , \tag{2.130}$$

we have that these $N_x - 1$ energy eigenstates for each θ_2 are grouped into q bands each with $(J-1)$ states, plus $(q-1)$ mid-gap states, which are the edge states. The condition $\big[M^J(\varepsilon)\big]_{21} = 0$ says that $M^J(\varepsilon)$ is a 2×2 upper-triangular matrix. It is satisfied by the simpler condition $M_{21}(\varepsilon) = 0$, which is an order $q - 1$ polynomial equation in ε, since any product of upper-triangular matrices is upper-triangular. It turns out that this condition sets the values of the $q - 1$ edge state energies, $\varepsilon = \mu_l$ with $l \in \{1, \ldots, q - 1\}$. The r^{th} edge state energy μ_j lies in the gap between bulk bands r and $r + 1$. Furthermore, since $\psi_0 = 0$ and we may choose $\psi_1 = 1$ (this is scaled by whatever normalization we may apply) for each r, we have

$$\psi^{(r)}_{kq+1}(\mu_r) = \big[M_{11}(\mu_r)\big]^k \tag{2.131}$$

and therefore we conclude

$$\begin{aligned} &\bullet \ \big|M_{11}(\mu_r)\big| < 1 \quad \Rightarrow \quad \psi^{(r)}_i \text{ localized on left edge } (i \approx 1) \\ &\bullet \ \big|M_{11}(\mu_r)\big| > 1 \quad \Rightarrow \quad \psi^{(r)}_i \text{ localized on right edge } (i \approx N_x - 1) \quad . \end{aligned} \tag{2.132}$$

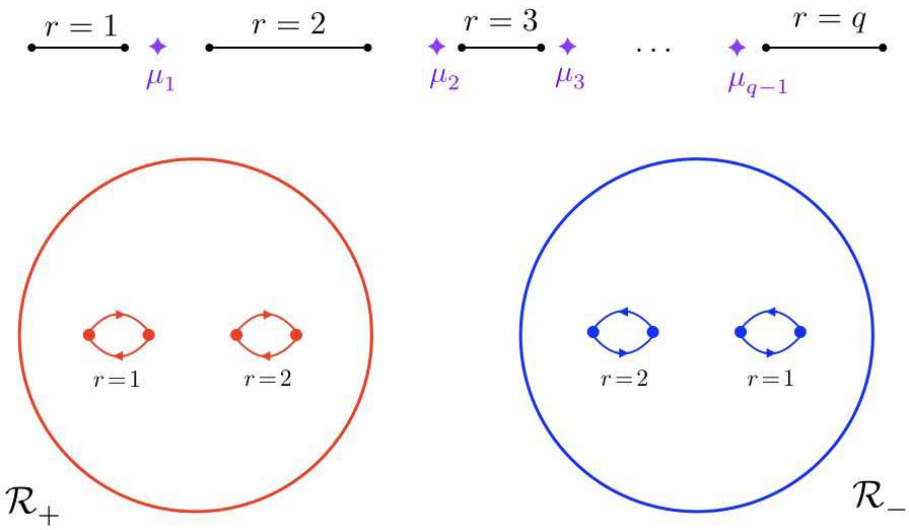

Figure 2.27: Hatsugai's construction of the genus $g = q - 1$ Riemann surface.

When $\left|M_{11}(\mu_r)\right| = 1$, the edge level merges with the bulk and there is no exponential localization.

With doubly periodic (*i.e.* toroidal) boundary conditions, the Bloch condition is

$$\begin{pmatrix} \psi_{q+1} \\ \psi_q \end{pmatrix} = M(\varepsilon) \begin{pmatrix} \psi_1 \\ \psi_0 \end{pmatrix} = e^{i\theta_1} \begin{pmatrix} \psi_1 \\ \psi_0 \end{pmatrix} \quad . \tag{2.133}$$

Following Hatsugai, we now analytically continue $\varepsilon \to z \in \mathbb{C}$ and we define the phase $\rho \equiv \exp(i\theta_1)$. Solving for $\rho(z)$, we have $\det\big(\rho - M(z)\big) = \rho^2 - T(z)\,\rho + 1 = 0$, where $T(z) = \mathrm{Tr}\, M(z)$. Note that $\det M(z) = 1$ since $\det R_n(z) = 1$ for all n. The solution is

$$\rho(z) = \tfrac{1}{2}\,T(z) \pm \tfrac{1}{2}\sqrt{T^2(z) - 4} \quad . \tag{2.134}$$

Furthermore, we have

$$\psi_0 = -\frac{M_{21}\,\psi_1}{M_{22} - \rho} \qquad \Rightarrow \qquad \psi_q = -\frac{\rho M_{21}}{M_{22} - \rho} = \frac{1}{M_{12}}\,\rho\,(\rho - M_{11}) \quad . \tag{2.135}$$

Define $\omega(z) = \sqrt{T^2(z) - 4}$. The branch cuts in $\omega(z)$ define the bulk energy bands, where $T^2(z) < 4$ and $z = \varepsilon \in \mathbb{R}$, which entails $|\rho(\varepsilon)| = 1$. Therefore, we can write

$$\omega(z) = \sqrt{(z - \lambda_1)(z - \lambda_2)\cdots(z - \lambda_q)} \tag{2.136}$$

where the $r^{\rm th}$ bulk band energies satisfy $\varepsilon \in [\lambda_{2r-1}, \lambda_{2r}]$. We may compactify, taking all values of z for $|z| \to \infty$ to a single point. The need to specify a sign for $\omega(z)$, which is a square root, means we have two spheres, $\mathcal{R}_+$ and $\mathcal{R}_-$, each with q branch cuts corresponding to the bulk

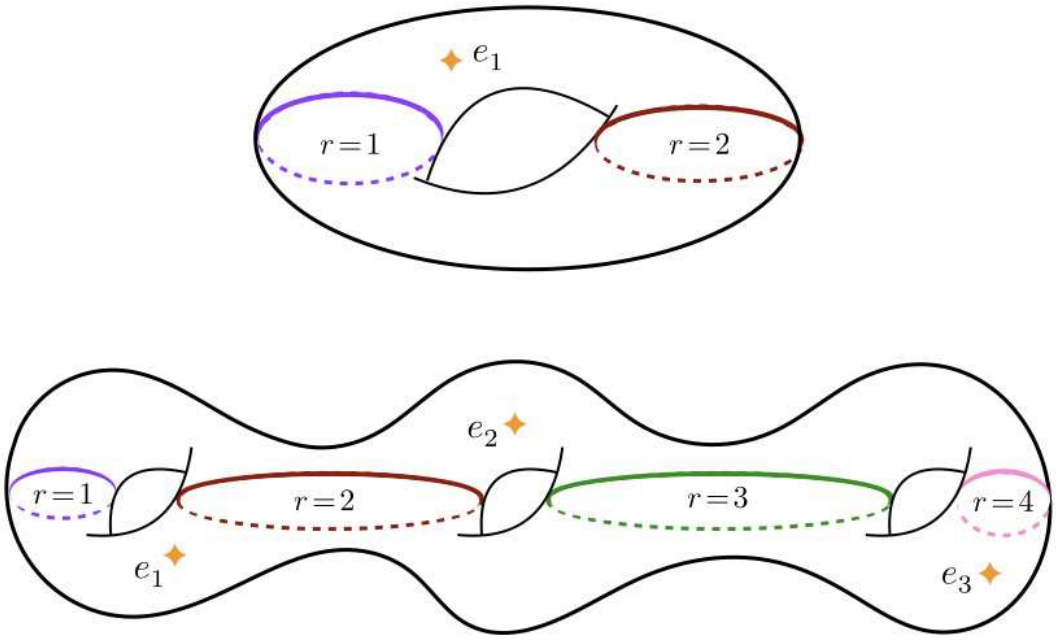

Figure 2.28: Genus $g = 1$ and $g = 3$ Riemann surface with q bulk bands and $q - 1$ edge states for each value of θ_2.

bands. The branch of $\omega(z)$ is defined such that $\omega(z \to -\infty) \gtrless 0$ on $\mathcal{R}_\pm$. The spheres $\mathcal{R}_\pm$ are glued together as shown in Fig. 2.27 to create a genus $g = q - 1$ Riemann surface, $\Sigma_g(\theta_2)$ for each θ_2, which is the complex energy surface for the Hofstadter model (see Fig. 2.28). Note that g is the number of gaps, and hence the number of edge modes.

Each edge state must satisfy $\psi_q^{(r)}(\mu_r) = 0$. There are g such solutions on $\Sigma_g(\theta_2)$. As θ_2 is varied, $\mu_r(\theta_2)$ moves around the $r^{\rm th}$ hole in an oriented loop. The winding number of this loop, I_r, determines the Hall conductance, with the Chern number of the $r^{\rm th}$ band being given by

$$C_r = I_{r-1} - I_r \qquad \Rightarrow \qquad \sigma_{xy} = \frac{e^2}{h} \sum_{j=1}^{r} C_j = -\frac{e^2}{h} I_r \quad , \tag{2.137}$$

where r is the label of the highest-lying filled band.

2.3.2 Qi-Wu-Zhang picture

Recall that the raisin bagel, while a culinary abomination and an outrageous form of cultural appropriation of my people, nevertheless furnishes a useful paradigm for the Wigner - von Neumann theorem, which says that accidental degeneracy for complex Hamiltonians has co-

dimension three[65]. The raisin bagel corresponds to a three-dimensional *filled torus*, parameterized by the two Bloch phases (θ_1, θ_2) and a third radial coordinate $r \in [0, 1]$. Degeneracies of two neighboring bands, $E_n(\theta_1, \theta_2, r)$ and $E_{n+1}(\theta_1, \theta_2, r)$, occur at discrete points $(\theta_1^*, \theta_2^*, r^*)$ within the bagel. We identify these points as the raisins.

In the picture of Qi, Wu, and Zhang[66] (QWZ), the radial coordinate r is a multiplicative factor in the hopping amplitudes on all links coupling sites with x-values N_x and 1. The Hamiltonian is taken to be

$$H = -\sum_{\langle \boldsymbol{R}\boldsymbol{R}' \rangle} \sum_{\alpha,\beta} \left(t_{\boldsymbol{R}\boldsymbol{R}',\alpha\beta}\, c^\dagger_{\boldsymbol{R}\alpha}\, c_{\boldsymbol{R}'\beta} + \text{H.c.} \right) + V \quad , \tag{2.138}$$

where V conserves local particle number $n_{\boldsymbol{R}} = \sum_\alpha c^\dagger_{\boldsymbol{R}\alpha}\, c_{\boldsymbol{R}\alpha}$ at every site $\boldsymbol{R}$, and may describe disorder or locally n-preserving interactions. On the links which straddle the horizontal and vertical "edges" Σ_{h} and Σ_{v} of the toroidal base space, we take

$$\begin{aligned} t_{\boldsymbol{R}\boldsymbol{R}'} &\longrightarrow r\, t_{\boldsymbol{R}\boldsymbol{R}'}\, \exp(i\theta_1 Q_1) \quad \text{horizontal edge} \\ t_{\boldsymbol{R}\boldsymbol{R}'} &\longrightarrow t_{\boldsymbol{R}\boldsymbol{R}'}\, \exp(i\theta_2 Q_2) \quad \text{vertical edge} \quad , \end{aligned} \tag{2.139}$$

where $Q_{1,2}$ are Hermitian matrices satisfying $\exp(2\pi i Q_j) = 1$, and where $t_{\boldsymbol{R}\boldsymbol{R}'}$ is for each link $\langle \boldsymbol{R}\boldsymbol{R}' \rangle$ a matrix with internal indices α and β, *viz.* $t_{\boldsymbol{R}\boldsymbol{R}',\alpha\beta}$ in Eqn. 2.138. Thus $H = H(\theta_1, \theta_2, r)$ has a three-dimensional parameter space, the filled torus, which interpolates between a cylinder at $r = 0$ and a torus at $r = 1$.

The Berry gauge connection for the n^{th} energy band is

$$A^{(n)}_\mu(\theta_1, \theta_2, r) = -i \left\langle\, \psi_n(\theta_1, \theta_2, r) \,\middle|\, \frac{\partial}{\partial \theta^\mu} \,\middle|\, \psi_n(\theta_1, \theta_2, r) \,\right\rangle \tag{2.140}$$

and the associated Berry curvature is

$$\Omega^{(n)}_{\mu\nu}(\theta_1, \theta_2, r) = \frac{\partial A^{(n)}_\nu}{\partial \theta^\mu} - \frac{\partial A^{(n)}_\mu}{\partial \theta^\nu} \quad . \tag{2.141}$$

At fixed r, integrating around a contour $\mathcal{C}$ on the (θ_1, θ_2) torus, one has

$$\Phi_n(\mathcal{C}, r) = \oint_{\mathcal{C}} d\theta^\mu\, A^{(n)}_\mu(\theta_1, \theta_2, r) \quad . \tag{2.142}$$

For notational clarity, we henceforth suppress the band index n.

[65] Seeded bagels are perfectly acceptable and indeed delicious. But bagels should not be defiled with cinnamon or sugar or fruit.

[66] X.-L. Qi, Y.-S. Wu, and S.-C. Zhang, *Phys. Rev. B* **74**, 045125 (2006).

In general, the connection cannot be defined globally, and instead only on patches. To this end, we define, for $r = 1$, $A_1^{\rm I}(\theta_1, \theta_2, r = 1) = A_1^{\rm II}(\theta_1, \theta_2, r = 1) = 0$, and

$$\begin{aligned} A_2^{\rm I}(\theta_1, \theta_2, , r = 1) &= \int_0^{\theta_1} d\theta_1' \; \Omega_{12}(\theta_1', \theta_2) \quad \text{for } \theta_1 \in (0, 2\pi) \\ A_2^{\rm II}(\theta_1, \theta_2, , r = 1) &= \int_{-\pi}^{\theta_1} d\theta_1' \; \Omega_{12}(\theta_1', \theta_2) \quad \text{for } \theta_1 \in (-\pi, \pi) \quad . \end{aligned} \tag{2.143}$$

Note the discontinuity in $A_2(\theta_1, \theta_2, , r = 1)$ at $\theta_1 = 0$ and $\theta_1 = \pi$. Thus, the (θ_1, θ_2) torus $\mathbb{T}^2$ is covered by two cylinders $\theta_1 \neq 0$ and $\theta_1 \neq \pi$. The Chern number is given by

$$C = \lim_{\epsilon \to 0} \frac{1}{2\pi} \int_\epsilon^{2\pi - \epsilon} d\theta_1 \, \frac{\partial}{\partial \theta_1} \left(\int_0^{2\pi} d\theta_2 \; A_2^{\rm I}(\theta_1, \theta_2, , r = 1) \right) \quad . \tag{2.144}$$

Following QWZ, we may define the quantity

$$\chi(\theta_1, r) \equiv \int_0^{2\pi} d\theta_2 \; A_2^{\rm I}(\theta_1, \theta_2, r) \tag{2.145}$$

and the phase $\Upsilon(\theta_1, r) \equiv \exp\bigl(i\chi(\theta_1, r)\bigr)$, so that

$$C = \frac{1}{2\pi} \oint_{r=1} d\Upsilon \; \Upsilon^{-1} = \frac{1}{2\pi} \int_{0^+}^{2\pi^-} d\theta_1 \, \frac{\partial \chi(\theta_1, r)}{\partial \theta_1} \quad . \tag{2.146}$$

Although $\chi(\theta_1, r)$ jumps by $2\pi C$ across $\theta_1 \in [0, 2\pi]$, the function $\Upsilon(\theta_1, r)$ is everywhere single-valued and well-behaved. Since $H = H(r\, e^{i\theta_1 Q_1}\, , \, e^{i\theta_2 Q_2})$, when $r = 0$ at fixed θ_2, the Hamiltonian is the same for all θ_1. Thus, (r, θ_1) may be viewed as 2D polar coordinates, with $r = 0$ the origin. It follows that if $C \neq 0$, there must be a vortex singularity somewhere within the unit disk $\{(r, \theta_1) \,|\, 0 \leq r \leq 1 \,,\, 0 \leq \theta \leq 2\pi\}$. Since $\chi(\theta_1, r)$ is well-defined provided the state $|\, \psi_n \,\rangle$ is nondegenerate, we conclude that one or both of the gaps $E_n - E_{n-1}$ or $E_{n+1} - E_n$ must collapse at some point in the interior of the disk if $C_n \neq 0$. Thus,

- ⋆ *Whenever $C_n \neq 0$ for the $r = 1$ system, there must exist one or more points $(\theta_1^*, \theta_2^*, r^*)$ with $r^* < 1$ where the state $|\, \psi_n(\theta_1^*, \theta_2^*, r^*) \,\rangle$ is degenerate with one of $|\, \psi_{n\pm1}(\theta_1^*, \theta_2^*, r^*) \,\rangle$.*

This is essentially a restatement of Wigner - von Neumann. Note that $r < 1$ corresponds to weakened inter-edge tunneling.